Safety Science 113 (2019) 472–489

Contents lists available at ScienceDirect

Safety Science

journal homepage: www.elsevier.com/locate/safety

Quantitative risk analysis for the Amerigo Vespucci (Florence, Italy) airport including domino effects

Iunio Iervolino[a], Domenico Accardo[b], Anna Elena Tirri[b], Gianmaria Pio[c], Ernesto Salzano[c,*]

[a] Dipartimento di Strutture per l'Ingegneria e l'Architettura, Università degli Studi di Napoli Federico II, Naples, Italy
[b] Dipartimento di Ingegneria Industriale, Università degli Studi di Napoli Federico II, Naples, Italy
[c] Dipartimento di Ingegneria Civile, Chimica, Ambientale e dei Materiali, Università di Bologna, Bologna, Italy

ARTICLE INFO

Keywords:
Aircraft dynamics
Aircraft crash risk
Infrastructure risk
Industrial risk
Cascading effects

ABSTRACT

Feasibility studies for airport facilities require quantitative assessment of the effects of the routine operations on the area surrounding the planned installation. In some countries such analyses are mandatory and the targets for which the effects need to be evaluated often include: cultural heritage, natural habitat, as well as human comfort and health. Regarding the latter issue, of main concern is the fatality risk due to airport traffic, primarily considering accidents due to landing and take-off operations. Accidents leading to crash may include fuel fires and explosions, but also trigger domino effects such as industrial accidents, possibly amplifying adverse consequences. Quantitative risk analysis for airport facilities is the topic of the study presented, where a probabilistic framework to evaluate the annual fatality risk for airports and surrounding areas is discussed. The risk metric is the *individual risk* (IR), and the methodology contemplates the tools and procedures to compute the annual expected number of accidents that result in fatality for each point in the area surrounding the airport. Three causes contribute to the evaluation of IR: (i) direct aircraft impact, (ii) heat radiation produced by the burning of fuel possibly released in the crash; (iii) heat radiation or intoxication because the crash involves industrial facilities storing or treating relevant amounts of hazardous materials. The risk analysis requires competencies mainly from three fields: (a) stochastic modelling for uncertainty management and probabilistic evaluation; (b) aeronautical engineering for the modeling of aircraft operations and dynamics that may result in an accident and, finally, (c) chemical engineering for the combustion modeling and for the analysis of cascading effects on industrial targets (also called *domino* in the following), as well as for the evaluation of health consequences. The developed method is thoroughly discussed in the paper and applied to the foreseen upgrade of the Florence (Italy) airport Amerigo Vespucci, which shows its potential effectiveness in decision making preparatory to airports' design.

1. Introduction

In recent years, important research efforts have been dedicated to innovative applications for Air Traffic Management or ATM. Original systems and procedures for ATM have been developed more than fifty years ago. Nowadays, they suffer from obsolescence, since several issues have arisen, such as the significant increase of worldwide traffic, the concern about flight security, the attention to the environmental impact of aviation, and the development of new transport systems that are direct competitors of aviation; e.g., high-speed trains. Finally, the integration of unmanned aircraft into non-segregated airspace introduced additional issues to be accounted for (Fasano et al., 2015). Airports are critical components of the ATM system for several reasons. They are the bottleneck of air traffic, since handling high volumes of landing and departing aircrafts often causes a slow-down of operations. Standing to statistics, most aircraft accidents happen in proximity of aerodromes because they are the place where all high-risk mission phases are executed, such as taxing, takeoff, and landing (Oster et al., 2013).

Large research programs have been developed worldwide to investigate the feasibility of solving ATM issues by exploiting new technologies and procedures, such as SESAR (EUROCONTROL, 2015) in Europe and NextGen in the U.S.; Coordination Committee (CCOM) for the US-EU MoC Annex 1 High-Level Committee, 2014. They all have developed projects to improve airport operations by exploiting advanced technologies. A main aspect to be investigated is the evaluation

* Corresponding author at: Dipartimento di Ingegneria Civile, Chimica, Ambientale e dei Materiali (DICAM), Università di Bologna, Via U. Terracini 28, 40131 Bologna, Italy.
E-mail address: ernesto.salzano@unibo.it (E. Salzano).

https://doi.org/10.1016/j.ssci.2018.12.019
Received 31 August 2018; Received in revised form 30 November 2018; Accepted 19 December 2018

of third-party risk for the area that surrounds an airport (Mahony, 2014). This is a type of study that is carried out when a new airport must be realized, or major changes are undertaken on an existing airport; e.g., runway increase of length or relocation. This study is required to assess if the new configuration implies a risk that can be considered acceptable for the communities dwelling the surrounding area. Even if all national regulations require to perform this study to get the approval for the changes, no standard procedure has been developed yet. In the United Kingdom, *public safety zones* have been introduced (Davies and Quinn, 2004) where the estimated individual risk (see Section 3 and Appendix A for more details and definitions) is larger than 10^{-5}. In those zones, new housing development is forbidden. In The Netherlands, also the *societal risk* is accounted by considering the population density (Hale, 2002). Both approaches are only related to the event of crash; they do not account for the propagation of the damage and domino effects, whose estimation requires the modelling of the accidental scenarios determined by the spill over of fuel from the airplane tanks, as well as the possible effects determined by the interaction of the propagation vector (heat radiation, overpressure) of the same scenarios with industrial facilities, located within or in the proximity of the airport, and characterized by the storage or the manipulation of large amount of hazardous materials (as defined, e.g. by the *Seveso Directive*; 2012/19/EU, 2012).

In summary, the current models have two main limitations, such as: (1) they aim at evaluating low probability events, as the fatality risk equal to 10^{-5} or less, by exploiting the existing statistics of accidents in proximity of the runway (Wong et al., 2009); however, the number of samples is generally small, and not necessarily adequate to model the specific facility in question; (2) they do not account for the possible propagation of the effects of the crash. Overcoming (1) requires the use of models for aircraft dynamics after a critical failure leading to crash during takeoff or landing. This model needs detailed information about aircraft configuration including inertial terms, aerodynamics parameters, fuel tank layout and crashworthiness, also accounting for uncertainties. All the terms must be provided for each aircraft that is included in the fleet mix of the airport so that the total risk can be estimated by weighting the risk of each aircraft by the relevant traffic share. Once the model has been developed, it can be exploited to estimate the geographic distribution of risk by means of numerical analysis specific to the facility of interest. Standing the capability to perform an adequate number of runs, the first limitation can be resolved. It also serves to overcome (2) as it allows estimating the average dynamics conditions of each aircraft at crash; i.e., horizontal and vertical ground speed. If crashworthiness information is available for the same aircraft, an immediate solution is given by verifying the type of damage determined for tanks and the resulting spill over conditions. These are the input information for the chemical risk engineering analysis, which enables to evaluate the domino effects of the crash.

The objective of the study is to discuss a framework for the calculation of the fatality risk in airport facilities and surrounding areas. The risk analysis includes the domino effects related to the presence of industrial facilities in the same area, which may be directly or indirectly involved in the crash. The risk metric is the *individual risk* (IR) defined as the annual risk (probability) of death for an individual who is continuously standing for three hundred and fifty-five days at a point in the area concerned. This risk index has been considered previously for airport risk studies (Hale, 2002) and also in other impact assessment studies of anthropic activities (De Waal et al., 2015). The consequences of the accident, which may cause conditions for a fatal outcome at any point in the area, are:

(a) direct (mechanical) impact of the aircraft;
(b) direct effect of energy radiation following the release of fuel (*leakage*) at the time of crash possibly triggering fires (*pool-* and *flash-fires*);
(c) indirect energy radiation (*domino/domino*) because the crash triggers a major accident in an industrial plant located in the area under study; the triggered incident may have fatal consequences as a result of the ignition/dispersion of the hazardous materials processed/stored in the facility.

The method is applied to the real case-study represented by the prospect extension project of the Amerigo Vespucci airport of Florence (Italy), for which a new runway of 2.4 km operating in one direction is designed to replace the current 1.7 km runway. Although the method presented in this paper could be applied to any type of any fleet mix, the application refers to Airbus A320™ aircraft, which has been selected mainly because it will perform about 70% of traffic in the future configuration of the Florence airport.[1]

In order to illustrate and discuss the developed methodology, the paper is structured such that an overview of the considered airport is given first. Then, the probabilistic formulation of the risk analysis (i.e., the stochastic model) is described. It takes into account the consequences (a–c) of the aircraft crash as listed above. This formulation allows to pass from the *critical failure* rate of the aircraft, during takeoff or landing, to the crash rate at any point of the area, and then to the fatality rate for the same point, that is the IR. Subsequently modelling the aircraft dynamics model for the in-flight failure and crash is discussed. This model also provides the extent of the area impacted by the crash. In addition, the aeronautical model provides the probabilities that crash results in any specific fuel leakage scenario. These (conditional) probabilities are input data for the following modeling that refers to the, possibly lethal, consequences of the ignition of the fuel released in the crash. Both the ignition of the formed puddle and the possible cloud of vapors are considered also in relation to the domino effects of the crash on, or close to, an industrial facility storing and/or processing hazardous materials. The paper ends with a discussion of final results presented in form of risk maps and the related conclusions, as well as a critical review the working assumptions made in this study (given in the Appendix A).

2. Upgrade of the Amerigo Vespucci Florence airport (master plan 2014–2029)

The risk analysis discussed herein is applied to the upgrade of the Amerigo Vespucci Florence (Tuscany region – Italy) airport. The current airport of Florence is located in Peretola, at the administrative limit of the municipality of Florence, with partial involvement of the territory of the neighboring municipality of Sesto Fiorentino. The airport has a single runway and a so-called *air-side* system, which also includes the control tower, the security gates, the aprons for aircraft, a passenger terminal, and the freight terminal. The current airport runway was originally built at the end of the 1930 and it was 1 km long. After several enlargements over the decades, it reached its current configuration in 2006, achieving the overall length of 1.75 km. The usable length for the landing run varies from 0.977 km to 1.455 km, for takeoff it is between 1.67 km and 1.60 km. The characteristics of prevailing winds and some topographic issues limit the usability of the runway. The main commercial aviation aircrafts operating in the airport are: Airbus A318/319; ATR 42-500; BAE Avro RJ 85, RJ 100; Bombardier Q400; Embraer E-Jets E170, E175, E190, E195; Let 410; Saab 2000. During 2014, 2,251,994 passengers were transported, with 37 destinations served and 33,976 total aircraft movements. Fig. 1 (left) shows the perimeter of the current airport configuration.

The company operating the airport has developed a master-plan in the next decade to warrant further development. In particular, the

[1] It is to note that other airport operations or possible accidents, such as refueling, could be integrated in the risk analysis; nevertheless, these are not considered herein as the main target is the risk in the areas surrounding the facility.

Fig. 1. Satellite view of the current airport layout (left) and layout after the planned upgrade (right).

operator intends to exploit the demand, which has been latent for decades, of international carriers hitherto penalized by discussed limitations of the runway, to serve markets that are not currently connected with the Tuscany region airport system, given the role of primary touristic/industrial destination for passenger and freight activities, which is offered by the city of Florence. In fact, the 2014–2029 master-plan forecasts an air traffic scenario for the year 2029 of 4.5 million passengers and 48,000 annual movements. The most important component of the masterplan, which includes complete refurbishment of the airport and substantial expansion, is the construction of a new runway, with a different orientation, that would replace the current one. The new runway will be unidirectional (two routes for take-off and one for landing) with length of 2.4 km and width of 45 m, allowing a theoretical maximum capacity of 22 movements per hour compared to the current 15 movements per hour. The length of the runway has been chosen because it is suitable for the Airbus A320/321 and the Boeing B737-800, which cannot now operate in the current configuration of the airport, while they are the reference aircrafts for the air carriers that are interested in the Florence destination in the near future. Fig. 1 (right) shows the prospective perimeter of the upgraded Amerigo Vespucci airport. It is relevant to note, and will be thoroughly addressed in the following that, beyond the fact that the airport is located within an urbanized area, it is surrounded in its vicinity, by three hazardous industrial installations as per the Seveso-directive (2012/19/EU, 2012).

3. Risk definition and stochastic modeling

The stochastic modeling for IR developed herein follows the principles of probabilistic risk analysis (e.g., Paté-Cornell, 2002). To compute the IR is assumed that the area of interest is discretized in a grid of points, each of which is analyzed individually. In fact, it is assumed that, at each point, a person is standing for one year continuously, without any protection (e.g., a shelter), possibly suffering lethal consequences due to a crash. In this logic, the point under analysis is a *target* of the crash effects (direct or indirect), while the points where crash can occur are *sources*. The probabilistic formulations aim at providing the framework to calculate the annual rate of accidents which cause death in the target point due to the consequence of a crash occurring at any other of the grid points. It will also be discussed in this section how to transform such a rate in a probability.

3.1. Rate of occurrence of critical failures and crash-rate map

The event initiating the possibly deadly consequences is the in-flight *critical failure* (i.e., fault) of the aircraft of interest during takeoff or landing. It is assumed that, a critical failure certainly results in a *crash* somewhere in the area (Section 4), while fatality can possibly follow the crash (as will be detailed below, the crashes that can cause deadly consequences are of three types).

For the aircraft of reference, it is assumed that it is available the rate (average number per million of take-off and landing operations) of critical failures. Such a rate can be easily converted in the rate of failures per year if the number of landing/takeoff operations in one year is available for the airport facility of interest (assumed time-invariant, to follow). The annual rate of critical failure is indicated as in the left-hand side of Eq. (1), where ν_L and ν_T are the rates of occurrence of critical failures for landing and takeoff, respectively.

$$\nu_{tot} = \nu_L + \nu_T \tag{1}$$

It will be discussed in the aeronautical model (Section 4) that the rate of critical failures is not necessarily constant across the landing and takeoff routes, in such a case, indicating as s the coordinate along such routes, the rate in each point can be computed, for example for landing, as:

$$d\nu_L(s) = \nu_L \cdot f_{S|CF,L}(s) \cdot ds \tag{2}$$

where $f_{S|CF,L}(s)$ is the probability density function (PDF) of the location of the critical failure (CF) along the landing (L) route, given that the aircraft is landing. An analogous equation can be written for takeoff.

Now, a location of coordinates $\{x, y\}$ is considered. It represents an elemental area of the region of interest (i.e., for which the risk analysis is carried out). The average number per year of crash events occur at that point is sought. This rate density, that can be indicated as $\nu_{C,L}(x, y)$, it can be estimated for landing as:

$$\nu_{C,L}(x, y) = \int_s P[C(x, y)|L, s] \cdot d\nu_L(s) \tag{3}$$

where $P[C(x, y)|L, s]$ is the probability that a critical failure occurring at s during landing results in a crash in $\{x, y\}$. Considering also takeoff, with analogous symbolism, the rate of crash in $\{x, y\}$ can be computed as:

$$\nu_C(x, y) = \nu_{C,L}(x, y) + \nu_{C,T}(x, y) \tag{4}$$

Then repeating this computation, it is possible to build the crash-rate map for the study region: i.e., $\nu_C(x, y), \quad \forall \{x, y\}$.

3.2. Individual risk (fatality rate) at any location

Assume now that there is a person in a point coordinates $\{w, z\}$; i.e., the target point. That person is assumed continuously at the point for three hundred and sixty-five days (i.e., one year). The objective of the risk analysis is to calculate the average annual number of events, which

can cause death, referred to as non-survival ($\bar{S}$), for the person located in that point. This rate, indicated as $\lambda(w, z)$, can be calculated multiplying the rate of crash at point $\{x, y\}$ by the probability, say $P[\bar{S}\,|x, y, w, z]$, of fatality in $\{w, z\}$ as a consequence of such a crash, then by summing (integrating) the obtained rates over the region:

$$\lambda(w, z) = \iint_{\{x,y\}} P[\bar{S}\,|x, y, w, z]\cdot\nu_C(x, y)\cdot dx\cdot dy \tag{5}$$

In this logic, the points $\{x, y\}$ are in fact the sources of deadly events for $\{w, z\}$. Aa it regards the term $P[\bar{S}\,|x, y, w, z]$, it in the framework of this study it is possible to distinguish three cases:

a. the crash point $\{x, y\}$ is sufficiently close to $\{w, z\}$ such as the cause of death is the direct impact form the crash;
b. the crash point $\{x, y\}$ is not sufficiently close to $\{w, z\}$ so that the crash directly impacts on it, and is not a point where a the crash can determine domino effects involving industrial facilities; in such cases, death can occur only by radiation of energy as a result of ignition of fuel leaked at the crash (see Section 5);
c. the crash point $\{x, y\}$ is not sufficiently close to $\{x, y\}$ so that the crash directly impacts on it, while it is a point where the crash can trigger domino effects on industrial facilities near-by, then death can occur because of radiation of energy following an accident that occurred in the affected facility as a result of the impact near to it (see Section 5.3).

In other words, when calculating the integral in Eq. (5) distinguish three types of points of crash $\{x, y\}$, which are schematically depicted in Fig. 2 and discussed in detail, from the perspective of the risk calculation, below.

3.2.1. Case (a): death by direct (mechanical) effect of the crash

Death by direct effect happens in case the point of coordinates $\{w, z\}$ is within the impact area. This happens if $r = \sqrt{(x-w)^2 + (y-z)^2} \leqslant r_C(x, y)$, where $r_C(x, y)$ is the radius of the crash impact area (to follow). Note that this radius may depend on the point of impact, because it depends on the trajectory of the aircraft. In this case it is reasonable to assume certain death: $P[\bar{S}\,|x, y, w, z] = 1$. Therefore, for a person in $\{w, z\}$, the rate of events that cause death by mechanical effect is:

$$\lambda_a(w, z) = \iint_{x,y:r\leqslant r_c} \nu_C(x, y)\cdot dx\cdot dy \tag{6}$$

3.2.2. Case (b): death due to the leaked fuel pool

If the point $\{w, z\}$ is outside the crash area, $r = \sqrt{(x-w)^2 + (y-z)^2} > r_C(x, y)$, and the crash area around $\{x, y\}$ does not contain a facility where a major industrial accident may occur (see, for example, Fabbrocino et al., 2005), then death in $\{w, z\}$ can occur only due to the effects of a pool of fuel possibly released during the plane crash. In fact, assuming that, whatever the point of the crash, there may be k (mutually exclusive and collectively exhaustive) aircraft fuel leakage scenarios $Leak_i(x, y)$, $i = \{1, 2, ..., k\}$, and assuming that the probability of death zero for no leakage, then the fatality rate can be written as in Eq. (7).

$$\lambda_b(w, z) = \iint_{\{x,y\}:r>r_c} \sum_{i=1}^{k} \{P[\bar{S}\,|x, y, w, z, Leak_i]\cdot P[Leak_i(x, y)]\} \times \nu_C(x, y)\cdot dx\cdot dy \tag{7}$$

For each leakage scenario (assumed mutually exclusive and collectively exhaustive along with the no-leakage case) the following chemical effects are considered:

(i) a pool fire of the accidentally released fuel;
(ii) a flash-fire (i.e., the fire of the dispersed vapor at concentration within the flammability range of the fuel) if late ignition is provided, followed by the pool fire as for the case (i);

In both cases, the pool fire scenario may possibly trigger an industrial accident via radiating energy towards an industrial facility located nearby of the flammable substances, or the release of toxic substances in the case of non-flammable substances. These two escalation phenomena (the industrial accidents) are considered as certain if the crash of the airplane occurs on the exact point of the same industrial equipment.

Because in case (i) the pool fire arrives before the industrial (domino) effect, it is possible to die for the latter only if one has survived the former. In case (ii) it is possible to die from the flash-fire, or, having survived it, it is possible to die by the delayed pool fire, or, if one survives even to it, death can be a consequence of the industrial domino eventually triggered by the crash. Therefore, in order to calculate $P[\bar{S}\,|x, y, w, z, Leak_i]$, it may be appropriate to refer to the event tree in Fig. 3, from which it is evident that the probability terms $P[\bar{S}\,|x, y, w, z, Leak_i]$ of each branch, needed to compute Eq. (7), are equal to the joint probability of all events of the nodes in the same branch:

$$P[\bar{S}\,|x, y, w, z, Leak_i] = \sum_{j=1}^{m} P[Branch_j\,|x, y, w, z, Leak_i] \tag{8}$$

As an example, the fatality probability due to domino effects in the case of flash-fire is discussed. It is the probability that the i-th-type leakage in $\{x, y\}$ forms a flash-fire (FF) to which the person in $\{w, z\}$ survives (S_{FF}), also surviving the following retarded pool fire (S_{PFR}) that follows. Conversely, the person does not survive ($\bar{S}_D$) the industrial domino (domino) triggered by the crash (D) in $\{x, y\}$. The sought joint probability can be obtained combining probabilities via the rule of multiplication of probabilities:

$$\begin{aligned} &P[FF \cap S_{FF} \cap S_{PFR} \cap D \cap \bar{S}_D\,|Leak_i] \\ &= P[FF\,|Leak_i]\cdot P[S_{FF}\,|FF, Leak_i]\cdot P[S_{PFR}\,|S_{FF}, FF, Leak_i] \\ &\times P[D\,|S_{PFR}, S_{FF}, FF, Leak_i]\cdot P[\bar{S}_D\,|D, S_{PFR}, S_{FF}, FF, Leak_i] \end{aligned} \tag{9}$$

In the equation, for simplicity, it is omitted the dependence $\{x, y\}$ and $\{w, z\}$ in the symbols.

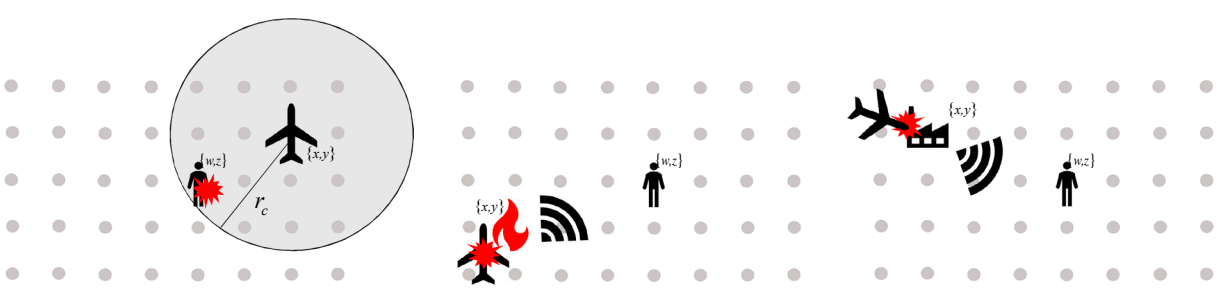

Fig. 2. Cases of crash points causing fatal events of type a (left), b (middle), and c (right), in $\{w, z\}$.

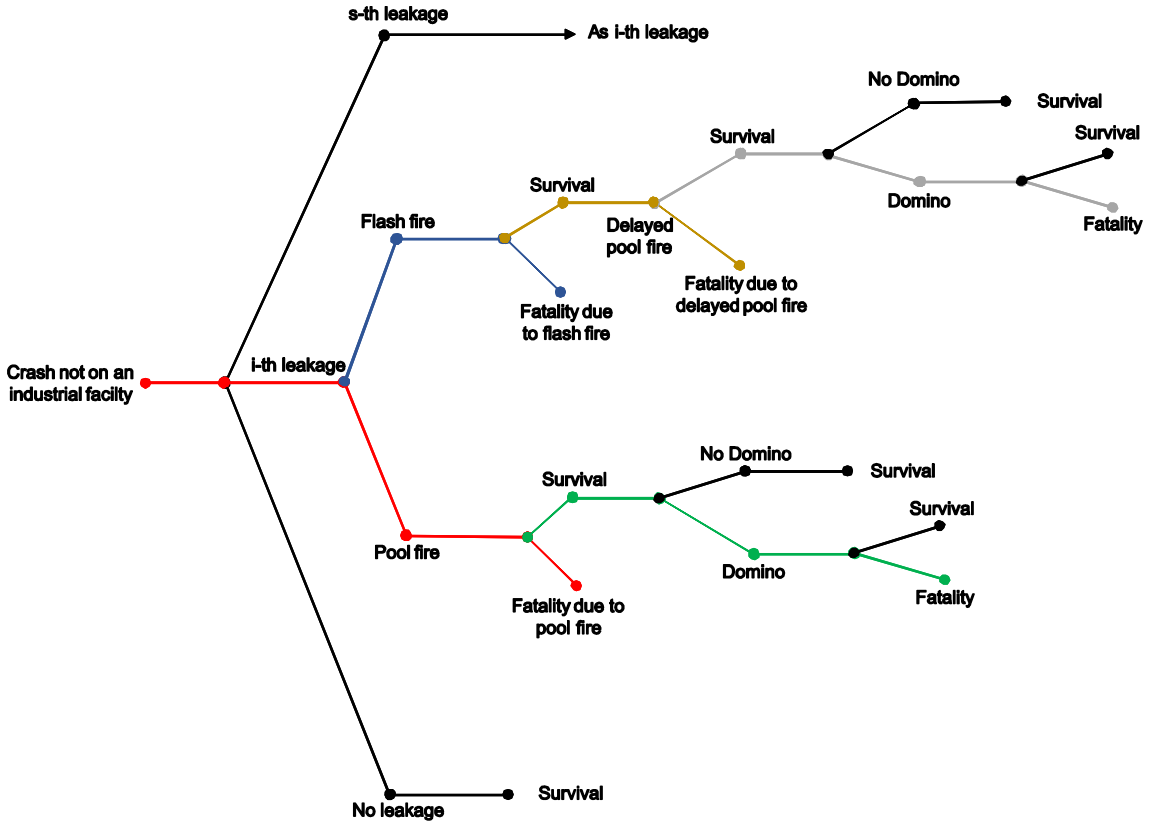

Fig. 3. Event tree in case (b) where the incident is not sufficiently near to cause death by impact, nor is it the place where a major industrial accident may occur.

3.2.3. Case (c): death as a result of industrial domino

If the incident involves a plant located directly in the impact area of a crash in $\{x, y\}$, then the fatality event rate in $\{w, z\}$ is computed by summing the crash rate at that point, multiplied by the probability of dying in $\{w, z\}$ because of an industrial accident triggered in the plant in question. If there are n industrial facilities treating hazardous materials, the contributions to the fatality rate in $\{w, z\}$can be computed as in Eq. (10), where $\{x, y\} \in I_i,\ i = \{1, 2, ..., n\}$:

$$\lambda_c(w, z) = \sum_{i=1}^{n} \iint_{\{x,y\}\in I_i} P[\bar{S} \mid x, y, w, z, i] \cdot \nu_C(x, y) \cdot dx \cdot dy \tag{10}$$

In case (c), to compute the probability $P[\bar{S} \mid x, y, w, z, i]$ it is necessary to consider that the crash causes fire to tanks containing the hazardous materials in the facility. This results in a pool fire of the tank's catch basin if the material is flammable. If the stored material is hazardous to health, the domino effect is toxic dispersion. Therefore, in the case of industrial domino, it is possible to die due to fire of flammable substances or release of toxic material substances that do not burn. As an illustration, see the event tree of Fig. 4, while please refer to Section 5.3 for details. (Note that second-order dominos, that this industrial accident triggered by the industrial accident following the crash, are neglected)

Finally, it is possible to get the fatality rate in $\{w, z\}$ via Eq. (11) for the cases type a, b, c, that can occur at any crash location $\{x, y\}$:

$$\lambda(w, z) = \lambda_a(w, z) + \lambda_b(w, z) + \lambda_c(w, z) = \iint_{x,y:r\leqslant r_c} \nu_C(x, y) \cdot dx \cdot dy + \iint_{\{x,y\}:r>r_c} \sum_{i=1}^{k} \{P[\bar{S} \mid x, y, w, z, Leak_i] \cdot P[Leak_i(x, y)]\} \cdot \nu_C(x, y) \cdot dx \cdot dy + \sum_{i=1}^{n} \iint_{x,y\in I_i} P[\bar{S} \mid x, y, w, z, i] \cdot \nu_C(x, y) \cdot dx \cdot dy \tag{11}$$

When computing the equation, it should be highlighted that each source $\{x, y\}$ should be considered only once. Also note that the equation does not give explicit evidence of the difference of risk calculation between takeoffs and landings. If needed, however, it is possible to split the IR calculation, distinguishing the rate of fatal accidents in the two maneuvers in question and then proceeding as just described for each of the two.

3.3. Individual risk

For any time interval, Δt, in which we could consider the fatality rate as a constant, the probability of death in $\{w, z\}$, $p(w, z)$, can be computed as:

$$p(w, z) = 1 - e^{-\lambda(w,z)\cdot\Delta t} \tag{12}$$

this is because if the rate is constant it is generally possible to treat it like a homogeneous Poisson process in which the time between two successive deadly events follows an exponential probability distribution (Benjamin and Cornell, 1970). Consequently, the IR can be computed assuming $\Delta t = 1$, which results in a probability figure similar to the fatality rate, if the latter is sufficiently small; i.e., $IR(w, z) = 1 - e^{-\lambda(w,z)} \approx \lambda(w, z)$. The procedure to compute the IR is summarized in Fig. 5, while the aeronautical and chemical engineering models needed are discussed in the next sections.

4. Aircraft dynamics

This section reports the dynamical model adopted in this paper to characterize the typical performance of an aircraft involved in a crash scenario during takeoff and landing maneuvers. Traditional crash analysis systems are focused on the determination of the geographic distribution of the impact probability (Ale and Piers, 2000). However, they do not produce any information related to the magnitude of the consequences and the area that is involved in the crash even if these terms are considered important by recent guidelines (Commission, 2015). Conversely, the model described herein has mixed dynamical

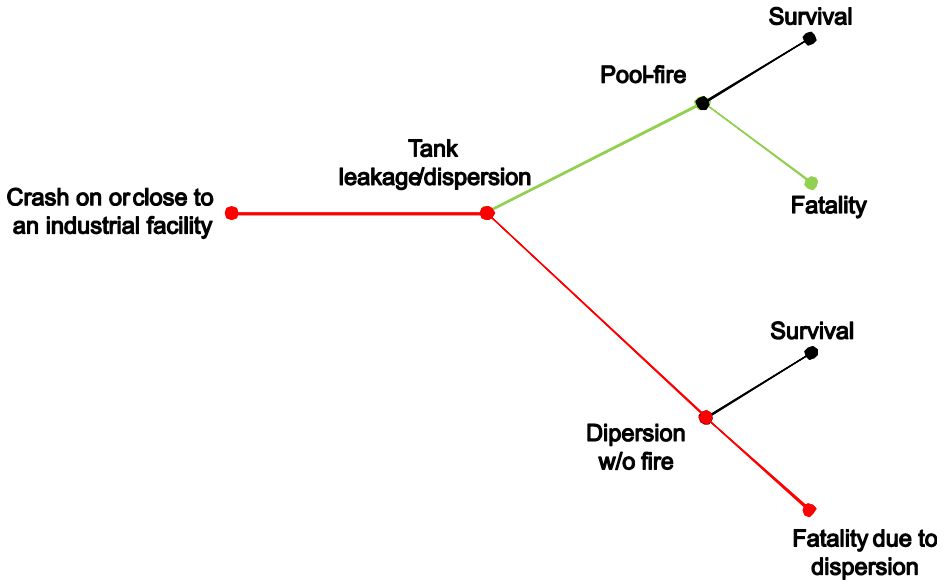

Fig. 4. Event tree in case (c) where the incident is not sufficiently near to cause death by impact, but it's the place where a major industrial accident may occur.

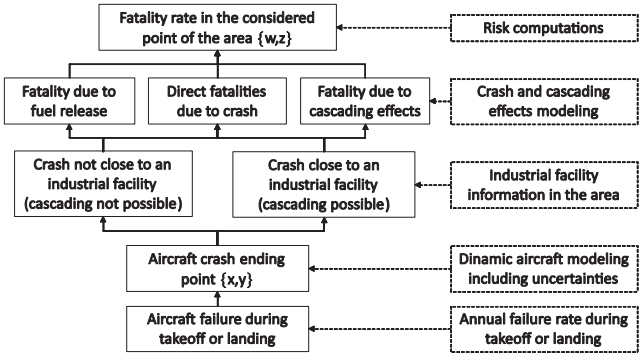

Fig. 5. Bottom-up flow-chart of the procedure to compute the individual risk and the needed aeronautical- and chemical-engineering models.

and probabilistic terms that allow to estimate several additional features, such as the probability of fuel leakage and the area of the impact surface.

The reference aircraft model employed is the Airbus A320™. Boeing 737™ and Airbus A320™ are the narrow body aircraft with the largest number of units manufactured (Reichmuth et al., 2018); moreover, they are in the short- and medium-haul category that is the largest share; i.e. 34%, in the overall worldwide fleet. Indeed, they are the typical planes adopted by low-cost airlines. Airbus A320™ has documented sources that describe the crashworthiness criteria adopted for the certification of fuel tanks (Airbus, 2005). Therefore, it is a representative aircraft for this kind of studies and it is also the reference aircraft for the case study of the Amerigo Vespucci airport. Nevertheless, the method can be generally applied to any type of aircraft or fleet-mix.

The main purpose of the models discussed in this section is to assess: (1) the geographical distribution of the probability of crash and fuel spillover over a region of interest surrounding an airport; and (2) the area of the surface affected by the crash as a function of the type of ground impact. As it regards (1), given the aircraft configuration reported in Fig. 6 (Airbus, 2005), three main tanks have been considered, such as the *outer tank*, the *inner tank*, and the *central tank*, and four leakage scenarios, $Leak_i$, $i = \{1, 2, 3, 4\}$ have been considered that have a significant probability to be verified in a real crash scenario:

1 - in the crash, no fuel spills out from the tanks;
2 - in the crash, the outer tank of one wing is affected by fuel leakage;
3 - in the crash, the fuel spills out from both the outer tank and the inner tank on the same side of the aircraft;
4 - fuel leakage from all the tanks (including the central tank).

It is worth noting that the combination of fuel leakage from opposite wing tanks, with no leakage from the central tank, is considered an event that as a negligible level of probability. This event could happen only in case of a perfectly symmetric crash.

4.1. Aircraft ground impact model

An aircraft dynamic model must be characterized to identify the aircraft path as soon as a critical failure occurs during takeoff and landing trajectories. In typical crash-landing conditions, the thrust is reduced, and the aircraft motion is produced only by the actions on aerodynamic control surfaces. This model is coherent with several aircraft accident models reported in the most relevant databases on aircraft accidents (FAA, 2017) and in standard procedures defined as forced-landing (FAA, 2016). The aircraft dynamic model can be expressed in the forward-up reference system by Eq. (13):

$$\begin{cases} m\frac{dV_H}{dt} + \frac{1}{2}\cdot\rho\cdot V^2\cdot S\cdot C_D - T = 0 \\ m\frac{dV_V}{dt} - \frac{1}{2}\cdot\rho\cdot V^2\cdot S\cdot C_L + m\cdot g = 0 \\ \frac{ds}{dt} = V_H \\ \frac{dh}{dt} = V_V \end{cases} \tag{13}$$

where: m is the aircraft mass at the time of critical failure; ρ is air density at altitude h; V_V is the vertical ground speed component; V_H is the horizontal ground speed component; V is the aircraft speed in absence of wind, that is the modulus of the vector-sum of V_V and V_H (the wind is considered as a random term whose parameters are extracted by local records); s is the along-route abscissa; h is the aircraft altitude in the forward-up reference frame with axes origin in the point of failure; S is the wing area for aerodynamic stress (not to be confused with survival in Section 3) computation and it is 122.6 m^2 for the considered aircraft (Nuic, 2017); C_D is the aerodynamic drag coefficient; T is the engine thrust (by associating crash condition to the one assumed for a critical landing phase – FAA, 2016 – it is assumed that $T \simeq 0$, which is a typical condition for landing, in case of overshoot and undershoot, and for takeoff with failure); C_L is the aerodynamic lift coefficient; g is the

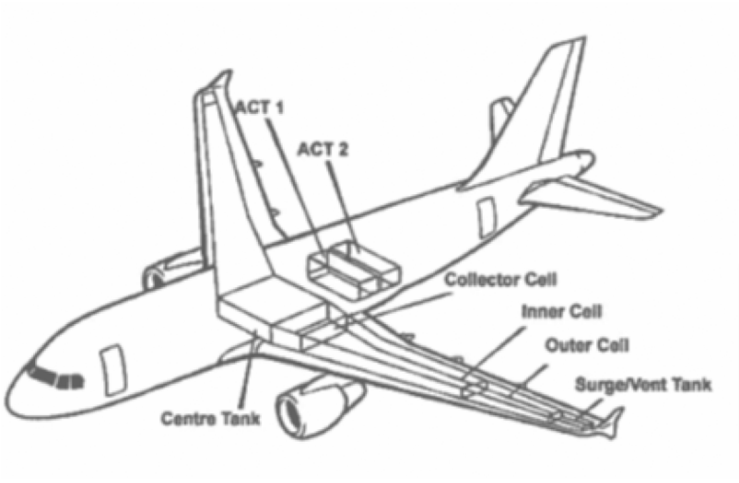

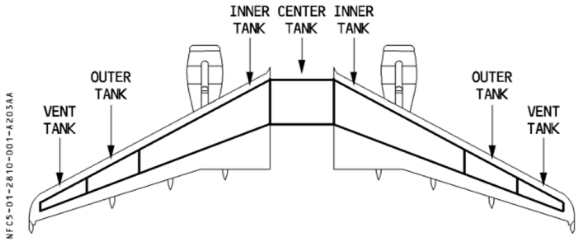

USABLE FUEL					
		OUTER TANKS	INNER TANKS	CENTER TANK	TOTAL
VOLUME	(liters)	880 x 2	6924 x 2	8250	23858
	(US gallons)	232 x 2	1829 x 2	2180	6302
WEIGHT *	(KG)	691 x 2	5435 x 2	6476	18728
	(LB)	1520 x 2	11982 x 2	14281	41285

* Fuel density : 0.785 kg/l or 6.551 lb/US Gal.

Fig. 6. Airbus A320 tank scheme and capacities.
adapted from Airbus (2004)

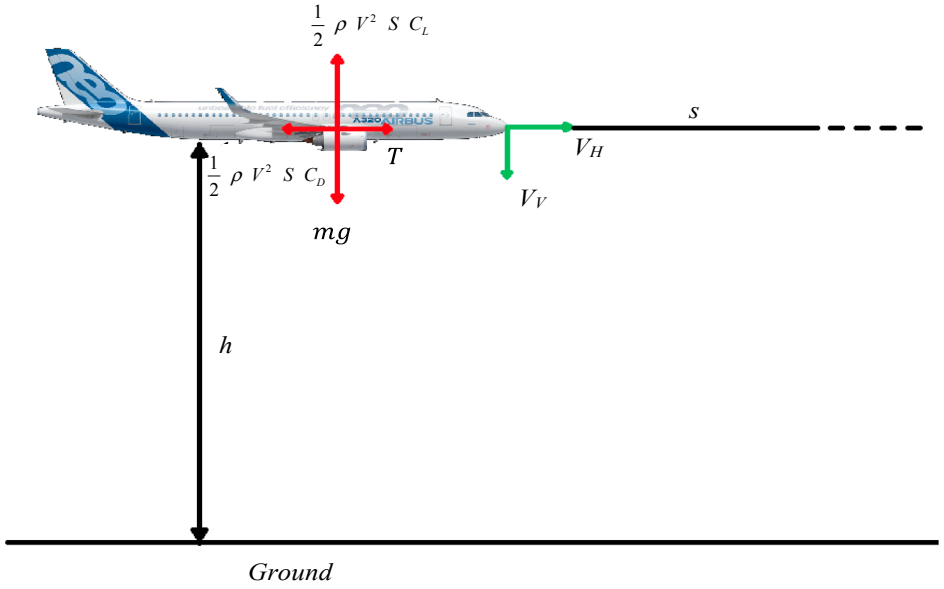

Fig. 7. Illustration of the reference system assumed for the aircraft dynamics.

gravity acceleration modulus (close to the ground it is equal to 9.81 m s^{-2}). The adopted reference system and reference terms are illustrated in Fig. 7.

The conditions at the time of failure ($t = 0$) are defined by Eq. (14), where h_0 is the altitude at the time of critical failure:

$$\begin{cases} V_V(t=0) = V_{0V} \\ V_H(t=0) = V_{0H} \\ h(t=0) = h_0 \\ s(t=0) = 0 \end{cases} \tag{14}$$

The terms C_D and C_L can be computed via Eqs. (15) and (16), respectively.

$$C_D = C_{D_0} + C_{DL} \cdot C_L^2 \tag{15}$$

$$C_L = \frac{2 \cdot m \cdot g}{\rho \cdot V_{H0}^2 \cdot S} \tag{16}$$

In the latter equation C_{D_0} is zero-lift drag coefficient; for the Airbus A320™ it is equal to $C_{D_0} = 0.038$ in case of flaps down and $C_{D_0} = 0.096$ in case of flaps down and landing gear extended (Nuic, 2017). C_{DL} is the lift-induced drag coefficient; for Airbus A320™ it is equal to $C_{DL} = 0.0419$ for flaps down and $C_{DL} = 0.0371$ for flaps down and landing gear extended.

It is assumed that after a failure the pilot tries to reduce vertical speed and avoid stall. To perform this type of correction the C_L value must be controlled by means of the aerodynamic control surfaces. Integrating Eq. (13), with the conditions given in Eqs. (14) and (17) results, where $a = 0.5 \cdot \rho \cdot S \cdot C_D \cdot m^{-1}$.

$$V_H(t) = \frac{V_{H0}}{1 + V_{H0} \cdot a \cdot t} \tag{17}$$

Similarly, the solution of the second equation in is (13) given by Eq. (18), where $k_L = 0.5 \cdot \rho \cdot S \cdot C_L$.

$$V_V(t) = V_{V0} - g \cdot t + \frac{k_L \cdot V_{H0}^2}{m} \left(\frac{t}{1 + V_{H0} \cdot a \cdot t} \right) \tag{18}$$

Integrating Eq. (13), the curvilinear abscissa can be derived as reported in Eq. (19).

$$s(t) = \frac{1}{a} \cdot \ln(1 + V_{H0} \cdot a \cdot t) \tag{19}$$

The solution of the fourth equation in (13) can be found by

integrating Eq. (20):

$$h(t) = h_0 + V_{V0}\cdot t - g\cdot\frac{t^2}{2} + \frac{k_L\cdot V_{H0}}{m\cdot a}[V_{H0}\cdot a\cdot t - \ln(1 + V_{H0}\cdot a\cdot t)] \quad (20)$$

Eq. (20) can be numerically solved to find the minimum time t^* that gives $h(t^*) = 0$. This is the time of the aircraft crash. Once t^* is calculated, it is possible to replace its value in Eqs. (17–19) to find $V_H(t^*)$, $V_V(t^*)$, and $s(t^*)$, that is the solution of the dynamic model. In particular, $V_H(t^*)$ is the aircraft horizontal speed at the time of the crash, which can be used to estimate the surface of the impact area and it is helpful for the longitudinal load factor at the crash; $V_V(t^*)$ is the aircraft vertical speed at the crash and it allows determining the vertical load factor at the crash; $s(t^*)$ is the ground distance covered by the aircraft between the time of the failure and the time of the crash.

4.2. Sources of uncertainty

To assess the effect of risk determined by an aircraft that is maneuvering in the terminal area of an airport, two important sources of uncertainty must be considered, such as the distribution of crash rate by phase of flight and the probabilistic fuel tank leakage model. These conditions are discussed in the following subsections.

4.2.1. Failure rate by phase of flight

As it results from statistical analysis (Boeing, 2015), the probability of crash landing of an aircraft can have significant variations depending on the flight phase. When an aircraft is flying in proximity of the ground, the capability of the pilot to react to a failure is affected by the small amount of time needed to avoid a crash. This condition must be properly modeled along the nominal landing and takeoff trajectories. Therefore, two terms must be defined: (i) a model derived from statistical records that defines the average value of the aircraft failure rate for each flight phase; (ii) a quantitative parameter for measuring the variation of the failure rate within a single flight phase. The latter term must be computed by exploiting the state terms derived in Section 4.1. Regarding the first term, the model is defined considering the distribution of the accidents in the various flight phases obtained from recent studies conducted by Boeing (2015) and Airbus (2017). The first column of Table 1 contains the frequencies of registered fatal accidents per phase of flight. The second column indicates the Airbus A320™ failure rate for a single flight phase. This value is obtained multiplying the total failure rate of $1.1{\cdot}10^{-7}$ and the values of the first column.

For the second term, the selected reference parameter is the time between the critical failure and the ground crash (*time-to-touchdown* or T2T). It is defined as the ratio between the distance-to-target and the closing speed. It is an effective term to describe the change of failure rate with a mission phase. Including this effect is very important for takeoff and landing conditions, since experimental data shows that most accidents happen when the aircraft is in proximity of the ground (FAA, 2017). This is the case of runway *overrun* or *undershoot*. T2T can be associated to the time t^* obtained from Eq. (20). In general, if T2T is smaller than 20 s, the pilot is assumed to have not enough time to control the aircraft and to prevent any type of accident (Spitzer et al., 2015). For this reason, in order to define a model for the variation of the failure risk, the failure rate as function of the time T2T is modeled as a second order rational function; the coefficients of the function are determined considering that the failure rate varies during takeoff and landing (increasing for landing and decreasing for takeoff) with a mean values equal to those reported in the second column of Table 1 (first and last line) until it reaches the cruise value for t^* equal to 20 s. The resulting condition is depicted in Fig. 8. In the context of this study, the abscissa in the figure has to be interpreted as the time since the take-off or the time to landing, and the figure provides, for these two operations, how the critical failure rate changes as a function of time.

Table 1
Failure rate estimates for Airbus A320 during the different flight phases (Boeing, 2015).

Flight Phase	Fraction of failures per flight phase	Failure rate per flight
Takeoff and Initial Climb	0.14	$1.50{\cdot}10^{-8}$
Climb	0.06	$7.50{\cdot}10^{-9}$
Cruise	0.13	$1.38{\cdot}10^{-8}$
Descent	0.03	$3.75{\cdot}10^{-9}$
Initial Approach	0.09	$1.00{\cdot}10^{-8}$
Final Approach and Landing	0.55	$6.00{\cdot}10^{-8}$

4.2.2. Fuel tank leakage model

A stochastic model that gives the probability distribution of fuel tank rupturing for each case considered in the introduction of Section 4 has been developed. The model reported in Section 4.1 allows for estimating horizontal and vertical ground speed at time of crash. Nevertheless, the rupture of fuel tanks is determined by the level of inertial loads; i.e., the acceleration, at time of crash. Ground speed at crash time and accelerations induced by crash can be associated by considering the expected time of extinction (dispersion) of kinetic energy and momentum at the time of crash. Several aircraft crash studies report that the characteristic time for the extinction of the non-negligible part of the aircraft momentum is 0.2 s (Arros and Doumbalski, 2007). Thus, knowing the vertical and horizontal impact speed components, dividing the velocities for the characteristic time it is possible to determine the average acceleration and the relevant average inertial loads. The regulation JAR 25.963(d) (EASA, 2007) requires that tanks that are not connected to aircraft fuselage shall have no damages (case 1), that is probability lower than 10^{-6}, for vertical inertial loads lower than 4.5 g, while the same requirement is increased up to 9.0 g for tanks that are installed in proximity of the fuselage (leakage scenario 4). An intermediate condition is considered for the leakage case 3 that is related to a threshold of 6.0 g. The relevant probability distributions can be derived by considering a cumulative normal distribution for each case with standard deviation equal to $1\ \mathrm{m\,s^{-2}}$. The considered threshold inertial loads and the associated V_V values are reported in Table 2 for each of the four leakage scenarios identified at the beginning of Section 4. Therefore, the probabilities of the events in each point of the impact area can be evaluated considering the probability distributions identified earlier and the conditions reported in Table 2.

4.3. Crash contours

This section provides procedure adopted to determine the rate of fuel leakage from a tank due to crash landing at a specified geographic point in the surrounding of an airport, given failure, which was indicated as $P[Leak_i]\cdot v_C(x, y)$ in Section 3. Given the conditions discussed in the previous sub-section, this term is related to the aircraft having an inertial load larger than the limit load that generates a damage for the tank. As reported in Table 2, the impact load is proportional to the vertical speed at the crash. Therefore, the rate of fuel leakage from a tank is proportional to the probability that the vertical speed at the crash exceeds a specific threshold. To evaluate the probability contours in the area of interest for each case reported in the introduction of Section 4, a specific processing algorithm was developed. First, all the nominal trajectories for landing and takeoff (to follow) were considered. They can be discretized into a sequence of points so that two subsequent points are separated by a constant travel time (a travel time of 0.1 s was considered sufficient). Subsequently, a landing crash trajectory can be considered for the selected point and the nominal value of the time of crash t^* can be computed by introducing initial conditions in terms of altitude and speed. Subsequently, the effect of the several sources of error must be accounted for by assessing the following terms: (1) the spatial scatter of the impact point; (2) the distribution of the vertical speed at the crash; (3) the area of the impact surface.

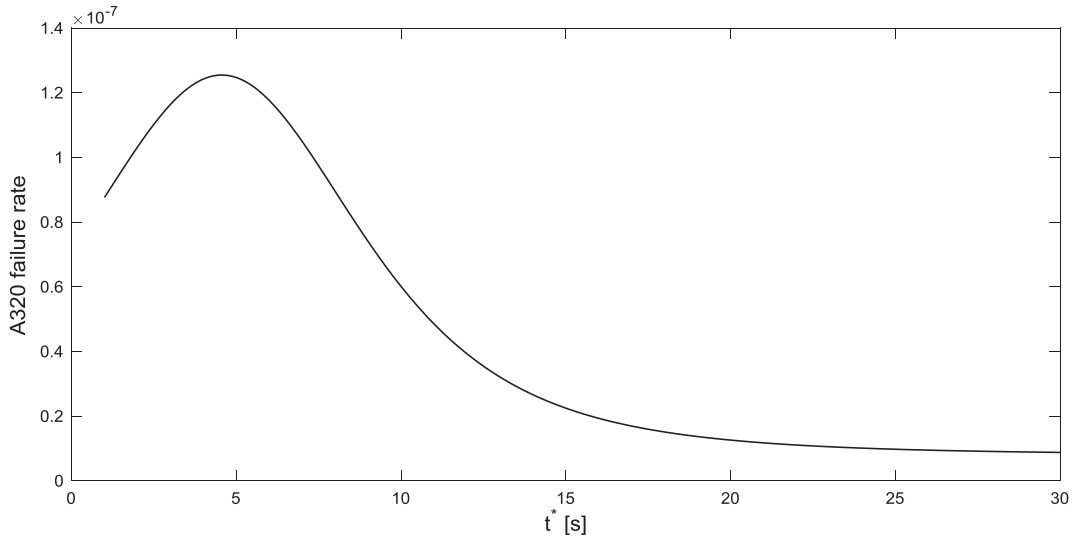

Fig. 8. Failure rate for A320™ as function of the touchdown time t^*.

Table 2
Inertial loads and V_V threshold values for the different events.

Leakage scenario: $Leak_i$	Inertial loads [g]	$V_V(t*)$[m s^{-1}]
i = 1	< 4.5	< 8.8
i = 2	> 4.5	> 8.8
i = 3	> 6	> 11.8
i = 4	> 9	> 17.7

The area surrounding the airport can be divided into a grid with relatively-fine spacing (e.g., 50 m) and the above reported terms can be estimated for each point of the grid as the position of the aircraft changes over the nominal landing and takeoff trajectories. The result of the above described process is a map of crash rates and a probabilistic distribution of the vertical speed at the time of crash per each point of the map. Consequently, the probability of each case reported in the introduction of Section 4 can be evaluated by combining the local crash probability and the fuel leakage probability for each tank computed as a function of the local distribution of vertical speed at crash. This map is the solution to the issues discussed in the introduction of Section 4. In the following subsections the criteria used to derive the terms reported in the list given in the previous paragraph are discussed to complete the description of the developed method.

4.3.1. Impact point determination

Several error sources affect the dynamic model defined in Section 4.1. In fact, the initial position (i.e., at the time of failure) can vary as function of the altitude and the cross-track coordinate due to aircraft navigation error. Moreover, the magnitude of the speed can be different from the nominal value due to a technical error during navigation or for the presence of a frontal wind component. Finally, the direction of the speed can be affected by an error in the estimation of the aircraft attitude or by the presence of a transversal wind component. Thus, once the most probable impact point is identified by means of the deterministic model, the variability of the impact point must be evaluated. Its distribution can be represented by a combination of radial and azimuthal displacement with respect to the nominal impact point. These distributions are modeled as two independent Gaussian distributions whose mean values are $\mu_\rho = s(t^*)$ for the radial component (determined with the dynamic model) and $\mu_\vartheta = 0$ for the azimuth component. The standard deviations of the distributions are given by:

$$\begin{cases} \sigma_\rho = \sqrt{\sigma^2_{\rho,nav} + \sigma^2_{\rho,wind}} \\ \sigma_\vartheta = \sqrt{\sigma^2_{\vartheta,att} + \sigma^2_{\vartheta,wind}} \end{cases} \quad (21)$$

where $\sigma_{\rho,nav}$ is the standard deviation of the range error caused by a navigation error (i.e., caused by the variability of the initial speed); considering this value as 0.1 of the nominal speed (ICAO, 2009), $s(t^*)$ can be evaluated for $1.1 \cdot V_{H0}$ and the resulting value can be detracted from $s(t^*)$ evaluated for the nominal V_{H0} to calculate $\sigma_{\rho,nav}$; $\sigma_{\rho,wind}$ is the standard deviation of the range error due to the wind; using the average annual value in the proximity of airport as reported by local meteorological records, this velocity can be added to V_{H0} and the standard deviation can be determined following a similar procedure as the one exposed at the previous step; $\sigma_{\vartheta,att}$ is the standard deviation of the azimuth error due to an error in the aircraft altitude (the FAA, 2012, 2012, sets this value at 3°); $\sigma_{\vartheta,wind}$ is the standard deviation of the azimuth error due to the wind (considering a wind speed as reported above, this value can be found as $\sigma_{\vartheta,wind} = \arctan(V_{wind}/V_{H0})$). Finally, a set of lateral and vertical displacements were considered to simulate a bivariate Gaussian distribution that represents the distribution of uncertainty for lateral and vertical displacements accepted by aeronautical authorities during takeoff and landing. The overall solution in a single trajectory point is given by the average of the solutions for each point. As an illustration, Fig. 9 gives the probability contours in case $\sigma_\rho = 100$ m and $\sigma_\vartheta = 10°$. The contour values are given in terms of ratio with respect to the maximum, which is at the (deterministic) impact point; i.e., (0,0) coordinates.

4.3.2. Uncertainty of the vertical speed at the crash point

As discussed above, the main purpose of the model is the determination of the probability that the speed components exceed a specific threshold value. The geographic distribution of the velocity components $V_H(t^*)$ and $V_V(t^*)$ must be mapped. This is carried out such as:

1) during the simulation, the takeoff and landing trajectories are divided in a set of points uniformly spaced in time; for each point, $V_H(t^*)$ and $V_V(t^*)$ are evaluated considering a crash landing trajectory as reported in Section 4.1 (the initial altitude and speed are set equal to the nominal value of altitude and speed in the selected point);
2) for each point of the trajectory, the probabilistic model described in the previous subsection is applied to find the dispersion model of the ground impact point;
3) the velocities determined at step 1 are employed for the evaluation

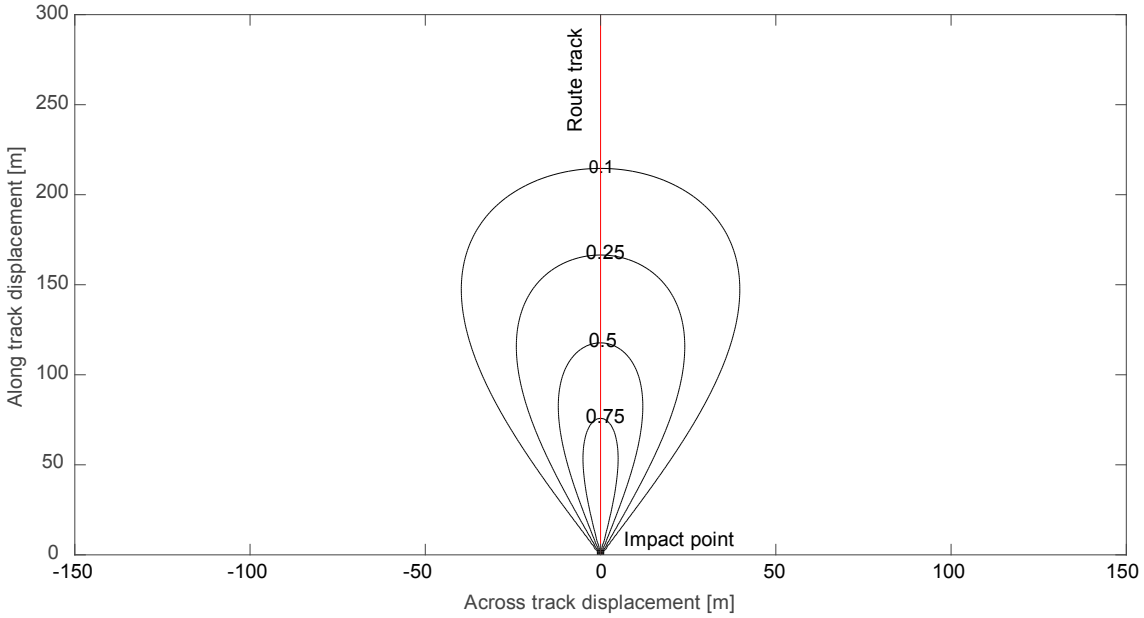

Fig. 9. Probability contours in case $\sigma_\rho = 100$ m and $\sigma_\theta = 10°$.

of the mean and standard deviation of the impact speed distributions (Gaussian); for each trajectory point, the impact speeds computed on ground points are weighted with the impact point probabilities determined at step 2, before being added to the values computed for other trajectory points to derive an overall estimate of the distribution of the impact velocities.

The result of the simulation result is the probability map for the impact velocity for all the points of the airport's surrounding area.

4.3.3. Evaluation of the impact surface area

The impact surface area can be evaluated as a function of the estimated stopping time for the aircraft after crash and the horizontal impact speed. The stopping distance s_{arr} is given by:

$$s_{arr} = \frac{[V_H(t^*)]^2}{2 \cdot g \cdot b} \tag{22}$$

where b is the dynamic friction coefficient; in case of relevant crash, it is set equal to $b = 0.99$. Multiplying this coefficient by the aircraft wing span, $l = 35.8$ m, the impact area can be evaluated. In general, this area can be increased by 10% to consider the distribution of debris. This area is used to determine r_C discussed in Section 3.

4.4. Crash and leakage scenario rates' results

At this point the annual crash rates, $\nu_C(x, y)$, contours evaluated with the described methodology can be given for the takeoff and landing maneuvers in the upgraded Amerigo Vespucci airport considering the 2029 traffic scenario, Fig. 10. It is to note that these rates are in the order of 10^{-8} at the maximum, reached close to the tip of the runway.

Note that in the same figure, the two takeoff routes (trajectories) designed for the airport upgrade are also given as the dark grey lines. Fig. 10 reports also a star for each position of industrial facilities considered in the risk analysis for the domino effects (to follow), which are indicated as facility (A), (B), and (C).

In the maps in Fig. 11 the results of the aircraft modelling are given in terms of 10^{-8} contours of the the annual leakage rate, in the case of takeoff for the four scenarios $P[Leak_i] \cdot \nu_C(x, y)$, $i = \{1, 2, 3, 4\}$ for the study area surrounding the airport. In Fig. 12 the same rates as in Fig. 11 are given for landing, which has a single route, also indicated in the figure. In this case the location of the maxima is within the runway, as expected.

In terms of spatial distribution of annual rate of crash (Fig. 10), the reported results agree with conditions described in traditional methods for both landing and takeoff phases (Ale and Piers, 2000; Davies and Quinn, 2004), if similar airports are considered with same level of traffic, single unidirectional runway, and type of takeoff and landing paths. Regarding the spatial distribution of annual rates of crash for each considered scenario $i = \{1, 2, 3, 4\}$, the following considerations are reported:

1) in case of takeoff (Fig. 11), worst case scenarios (large values of i) are more frequent at large distance from runway, since these scenarios are determined when the aircraft kinetic energy at impact is larger (i.e., the aircraft has reached a high altitude);
2) in the case of landing (Fig. 12), a condition similar to that reported in the previous item is determined; therefore, accidents on runway are less likely to produce severe leakages.

It is worth noting that, even if the region where the annual rate of crash for the case $i = 4$ is more than 10^{-8} is large in the two figures, the overall probability for this event is much less than the case $i = 1$ that is more frequent when the aircraft is flying in proximity of the runway. This fact can be easily recognized if the overall crash rates distribution is considered (Fig. 10).

5. Consequence analysis for the fuel leakage

As extensively discussed, the airplane crash may produce a leakage from the fuel tanks. Three leakage scenarios with different mass of fuel released on the ground have been considered, in dependence of the type and number of affected airplane tanks. The released fuel, in certain conditions, may ignite and burn, thus evolving in combustion-related accidental scenarios (primary scenarios). These fires may in turn trigger further accidental scenarios (domino effects) if involving industrial installations located in the nearby of the airport site or however along the airplane route.

In this sub-section the chemical-engineering models to compute either the primary accidental scenarios related to the fuel leaked from the airplane after the crash or the domino effects are discussed, starting from the chemical characterization of the jet fuel. Both are considered

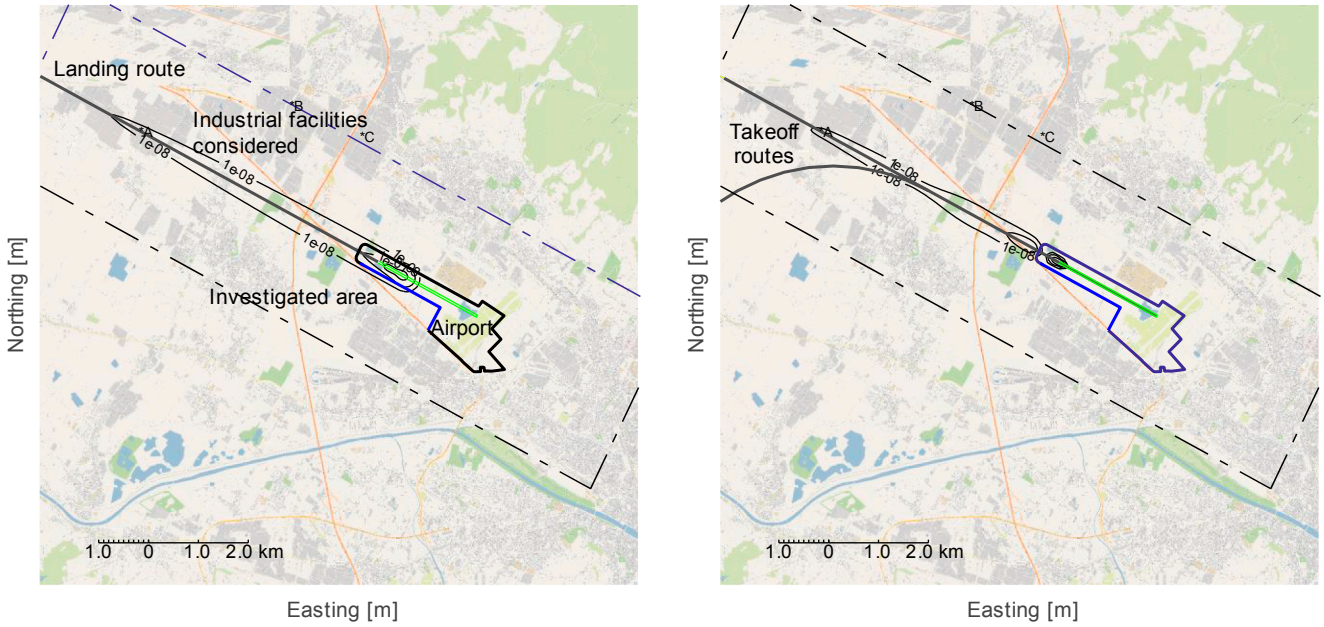

Fig. 10. Contours of annual rates of crash in the Amerigo Vesupucci airport area (dashed line) during landing (left) and takeoff (right) per the 2029 scenario.

as contributors to the IR as described in Section 3.

5.1. Fuel characterization

For what concerns the choice of the reference aircraft fuel, it is worth noting that several jet-fuel compositions are possible, because they may vary with the departure airport, the company nation and other factors (ASTM, 2010). In this study, a surrogate kerosene mixture containing the maximum, allowed quantity of aromatics compounds (25% volume) and n-alkanes (75% volume) has been considered and defined as JetA-1 (Table 3). This methodological choice allows the simulation of accidental scenarios involving the oxidation of Jet A-1 in air (combustion) on the safe side,[2] due to the typical higher reactivity (i.e., burning rate and heat of release rate) of aromatic substances with respect to other hydrocarbons (Glassman and Yetter, 2008).

5.2. Primary scenarios

The leakage of fuel from the storage system installed on the airplane, or alternatively the quasi-instantaneous release of the total amount of fuel due to the rupture of the shell of one or more tanks constituting the storage system of the vehicle (see Section 4), determines a liquid pool on the ground, followed by either early or delayed ignition. In both modalities, if the thermochemical conditions are matched, the fuel vapor formed over the liquid surface burns. In case of immediate ignition, the resulting fire is called *pool fire*. If a delayed ignition is provided, the dispersion of the fuel vapor in the atmosphere may produce a vapor cloud, which enlarges its volume with time due to evaporation rate, air entrainment and other dispersion phenomena.

For longer time, a steady state is reached between the fuel mass flow (the evaporation rate is mostly constant) and the air dilution, hence the section of the vapor cloud reaches a maximum in terms of volume and distance from the pool. The delayed ignition of the fuel vapor at any location, typically assumed at the edge, produces a flame which propagates along the entire section of the cloud with fuel concentrations within the flammability limits (i.e., the *deflagration*), followed by convective/diffusive flames of the fuel. The velocity of the flame propagation (the flame speed) may vary from few meters per second – in the first instants after the ignition – to higher velocity, up to hundreds of meters per second, in dependence of the fuel reactivity, dimensional scale, and congestion level (i.e., the *turbulence*). If the flame accelerates, the combustion wave may be able to produce destructive pressure waves even at large distances. In this case, the phenomenon is called *vapor cloud explosion* (VCE). On the contrary, the combustion wave is only observed, and the overall phenomenon is called *flash-fire*. Both flash-fire and VCE are followed by the pool fire, as they ignite the vapor over the liquid surface. Additional detail regarding consequence analysis assumption could be found in the current literature (CCPS, 2010; Mannan, 2012).

In this study, the VCE has not been considered, mainly because of the relatively low reactivity of fuel, which is typically measured in terms of laminar burning velocity, that is the flame velocity with respect to the unburnt gas. Indeed, at least in accidental conditions, it is likely that the entire cloud is characterized by non-homogenous fuel concentration due to the relative density of the vapor with respect to air and due to the formation of fuel mass concentration gradient, either horizontally or vertically for the effects of air entrainment and wind. These observations imply that only a fraction of the fuel vapor is within the flammability range, and that an even smaller portion of the fuel-air mixture is close to stoichiometric concentration, hence at higher reactivity. Furthermore, the high boiling point – or alternatively the low vapor pressure – of Jet A-1, despite conservative choices on its composition, induces a very low evaporation rate, with strong effects of dilution by atmospheric air and wind. These effects, together with the low probability of a delayed ignition in the presence of severe airplane crash, concur to generate a relatively small cloud, with consequent low amount of released flammable vapors (i.e., energy), and however to the restriction of the unlikely shock waves to the immediate surrounding of the cloud only. Finally, the low level of congestion in the airport track areas does not allow the flame acceleration due to obstacle-induced turbulence. Hence, only pressure waves with negligible ability to produce damages in the far field are generated. In the following, the pool fire and the flash-fire phenomena have been only analyzed.

5.2.1. Pool fire

Pool fires are represented as an inclined cylindrical flame over the fuel liquid surface, characterized by the fire diameter (D_F), commonly

[2] Although in risk analysis conservative assumptions are to be avoided as much as non-conservative assumptions (e.g., Erto et al., 2016).

Fig. 11. Contours of annual rates of leakage in the Amerigo Vesupucci airport area during takeoff.

assumed equal to the pool diameter (D_P), the flame height (H_F) and the tilt angle (θ); Fig. 13. Starting from this simplified geometry, the thermal radiation can be estimated by surface emitter model, considering the surface emitting power (*SEP*) magnitude proportional to the flame temperature (T_F), the emissivity (ε) and the Boltzmann constant (σ), as described by the Boltzmann law:

$$SEP = \sigma \cdot \varepsilon \cdot T_F^4 \tag{23}$$

Several empirical and semi-empirical models to estimate the geometrical dimensions of the pool fire cited above, the thermal radiation and the burning rate are presented in the current literature (e.g., Hottel, 1959, Babrauskas, 1983). On this regard, the Hottel plot, as reported by Drysdale (2011), is commonly adopted for the description of pool fire with respect to the pool diameter Fig. 13, right.

Starting from data reported in Fig. 13, right, several empirical rules were developed. The commonly accepted correlation is the Thomas equation (Babrauskas, 1983):

$$\frac{H_F}{D_F} = c_1 \cdot w^{c_2} \cdot \left(\frac{m''}{\rho_a \cdot \sqrt{g \cdot D_P}} \right)^{\frac{2}{3}} \tag{24}$$

where w stands for a constant depending on the wind speed, c_1 and c_2 are constants for a given fuel-oxidant mixture, ρ_a for the air density and g for the gravity acceleration. The mass burning velocity per unit surface (m'') can be calculated as in the following:

$$m'' = m''_\infty \cdot (1 - e^{-k \cdot \beta \cdot D_P}) = \frac{\sigma \cdot T_F^4}{\Delta H_\nu} \cdot (1 - e^{-k \cdot \beta \cdot D_P}) \tag{25}$$

where m''_∞ represents the mass burning velocity for infinite pool diameter, whereas k and β are constants (for kerosene: 2.60 m^{-1} and 1.35, respectively).

Fig. 12. Contours of annual rates of leakage in the Amerigo Vesupucci airport area during landing as per the 2019 scenario.

Table 3
The fuel composition and related physical and chemical characterization adopted in this study.

Fuel name	Jet A-1
Composition	75%v n-dodecane + 25%v toluene
Liquid density	806 kg m^{-3}
Boiling temperature	147 °C
Heat of vaporization	251 kJ kg^{-1}
Heat of formation	501 kJ kg^{-1}
Heat of combustion	37,500 kJ kg^{-1}

It is worth noting, however, that large scale experiments are not always available, in particular for the Jet A-1 fuel (Eddings et al., 2005). Therefore, empirical models are questionable. Hence, *computational fluid dynamics* (CFD) coupled with the *large eddy simulation* (LES) model for turbulence are applied to assess the evolution and the thermal effects of the pool fire. In this study, the *fire dynamic simulator* (FDS) developed by US EPA has been adopted. This code has been extensively validated and is commonly used for pool fire scenarios (Wen et al., 2007). Details are not reported here for the sake of brevity and can be found elsewhere (McGrattan and Miles, 2016). The FDS code is able to simulate the radiating heat with respect to the distance.

5.2.2. Flash-Fire

The flash fire phenomenon is intrinsically related to the dispersion of fuel vapor prior to the ignition. The dispersion analysis, quite clearly, depends on the evaporation rate and on the meteorological conditions, in terms of wind, atmospheric temperature and atmospheric stability. Following well-known procedures and standard analyses (CPR14E, 2005; CPR16E, 2005; CCPS, 2010; Mannan, 2012), two Pasquill/wind

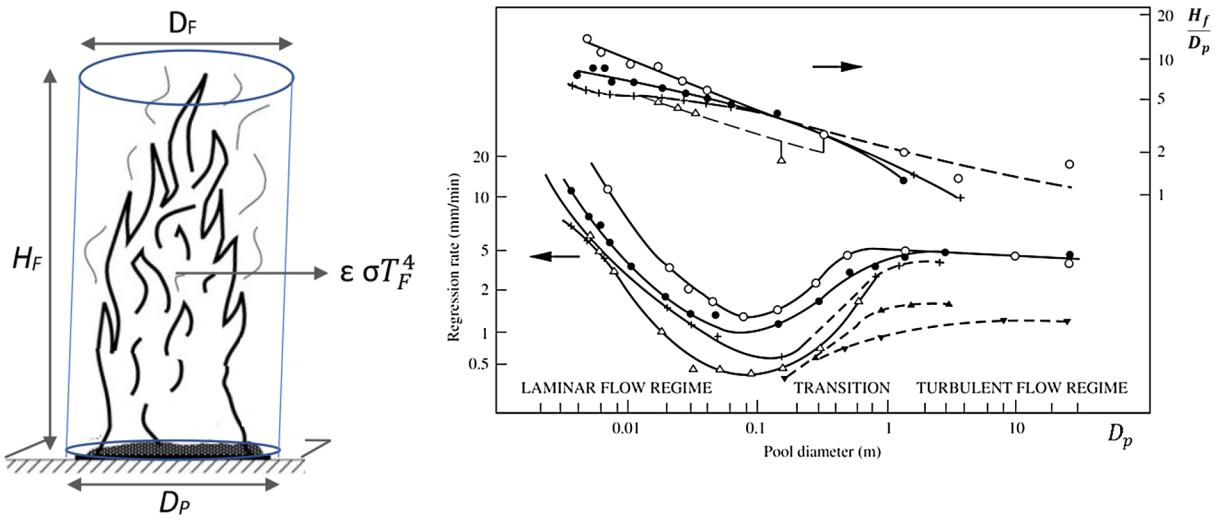

Fig. 13. Left: schematization of the pool fire scenario (CCPS, 2010); Right: Hottel correlations for pool fire in the terms of regression rate; i.e. the volumetric loss of liquid per unit surface area of the pool in unit time (equivalent to the burning rate) and flame height with respect to the pool diameter for different fuels as reported by Drysdale (2011). ○ Gasoline; ● Kerosene; Δ Solar oil; + Diesel oil; ▲Petroleum oil; ▼Mazut oil.

atmospheric conditions, D5 and F2, are only considered as reference atmospheric conditions for the dispersion analysis of the vapor from the source point. These two conditions are commonly considered as representative of the entire set of possible atmospheric conditions and describes the neutral atmospheric condition, typical of the day-time, with a wind velocity of $5\,m\,s^{-1}$ and the moderately stable conditions, typical of night-time with wind velocity of $2\,m\,s^{-1}$, respectively. An important point needs however to be clarified: the aviation fuel is intrinsically a high boiling liquid with flash point (i.e., the minimum liquid temperature for the formation of flammability of vapors) greater than 35 °C, and typically between 45 °C and 50 °C (ASTM, 2010). These conditions may be reached in daytime only. Hence, the Pasquill stability class, which occurs in night-time and with high cloudiness has not analyzed in this study.

The methodology here developed has adopted a circular vapor cloud with the radius corresponding to the maximum distance reached by the cloud along the wind direction, having considered a threshold concentration corresponding to the half (1/2) that of the *lower flammability limit* (LFL), that is the minimum concentration for the flame propagation to be observed at given temperature; a D5 conditions; and an ambient temperature of 45 °C, i.e. higher than the *flash point* of Jet-A1 composition adopted in this work (calculated as $T_F = 38$ °C).

Under these assumptions, the dimension of the cloud can be calculated either by simplified models or more complex tools, by using dispersion analysis for heavier-than-air vapor models (Blackmore et al., 1982). For the purposes of this analysis, it has been considered that lethality conditions are satisfied at all points of the cloud having concentration greater than the LFL, according to a widespread practice. This due to the high temperature of combustion gases (the products of combustion), which makes negligible the effects of thermal radiation in-stationary conditions. Conservatively, however, it was considered the certain lethality when fuel concentration is greater than half of LFL, which is the standard threshold value for the injuries.

5.3. Secondary scenarios (domino effects)

The primary scenarios considered, that is pool fire and flash-fire, may trigger secondary scenarios due to the interaction with industrial structures storing/treating significant amount of hazardous substances (Cozzani and Salzano, 2004a, 2004b). These accidents are commonly named domino effects (Salzano et al., 2013; Paltrinieri et al., 2013).

Herein it is assumed that the domino effect is only possible if the intensity of the thermal radiation exceeds a threshold value, which – based on long-term observation and physical considerations – has been associated to a level of structural damage to the equipment that, in turn, enables the secondary scenario (Cozzani and Salzano, 2004c). In this light, it is worth noting that flash-fire is generally excluded from domino effect analysis because of short duration of this phenomenon (Campedel et al., 2008).

The assessment of domino effect is than performed by creating a list of more hazardous plants at first, as recognized by Seveso Directive in Europe (2012/19/EU, 2012) or COMAH in UK (COMAH, 2015), together with the relative list of hazardous materials and corresponding amount of potentially hazardous materials which can be involved in the domino scenarios. The consequence analysis and the estimation of the damage distances for the secondary scenarios can be finally carried out by using the same fire and dispersion models described in the previous sections regarding the primary domino scenarios. In this study, an instantaneous release due to catastrophic rupture of industrial equipment, and an instantaneous ignition of the stored fuels (hence neglecting VCE, which requires unlikely late ignition) have been considered for all defined industrial installations in the surrounding of the airport when involved in the aircraft crash. If liquified flammable gases are of concern, such as *liquified petroleum gas* (LPG) the fireball scenario, that is the fire of the vapor phase of the boiling liquid, has been also considered. In this case, the classic equation of *Roberts* for the extension (diameter) of the *fireball* has been considered (Mannan, 2012). For this same type of substances, jet fire has been not considered due to assumption of catastrophic rupture of the involved equipment.

5.4. Results of the chemical modelling for the primary scenarios

With reference to the Airbus A320™ storage system, three different scenarios have been individuated and studied in detail, starting from the leakage assumptions (1–4) described in the previous section.

1 - No fuel spills out from the tanks: no accidental scenarios.
2 - In the crash, the outer tank determines liquid fuel spill of 691 kg. It may occur either in landing or in the take-off, in the case of a partial rupture of the tank.
3 - During the crash, the fuel spills out from both the outer tank and the inner tank on the same side of the aircraft: a release of fuel for 6126 kg has been considered. It may occur either in taking off or landing.
4 - Fuel leakage from all the tanks (including the central tank). A total spill of 18,728 kg is considered. It may occur only during take-

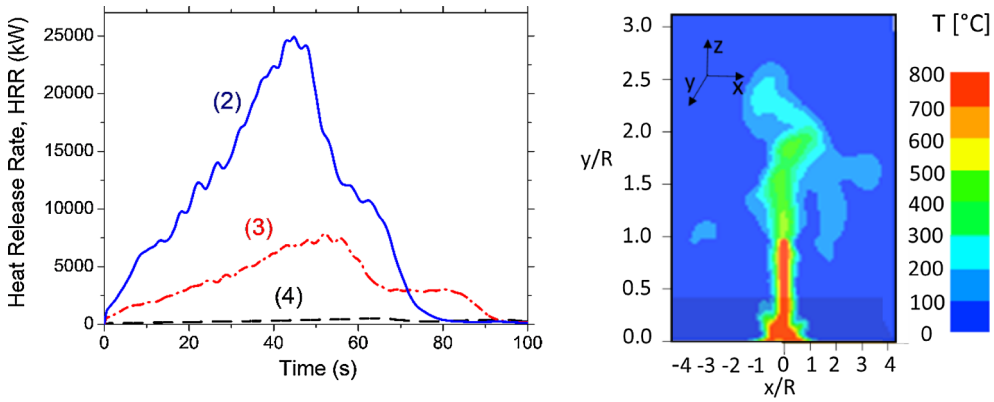

Fig. 14. Heat release rate vs time for the three pool fires analyzed, derived from the three leakage scenarios described above (left) and temperature profile (at flashover time) for the 6126 kg spill scenario (right). *R* is the pool radius.

off.

The aviation fuel spreading can occur on asphalt (landing and take-off ways; areas surrounding the airport) or on porous material as the braking area or earth ground around the airport line). The effect of pavement surface on pool depth was evaluated by considering the absence of any bund or slope and assuming a liquid cylindrical shape with 1 cm thickness as described in the *Yellow Book* (CPR14E, 2005). The calculated pool extension is the input data for the simulation of pool fire and flash-fires via FDS. For the early ignition scenario, a hotspot giving an amount of energy of 3 mJ, corresponding to the minimum ignition energy of Jet A-1, as reported by ASTM (2010), was set at the center-point of the vapor layer over the liquid pool.

Fig. 14 reports the calculated *heat release rate* (HRR) for the three analyzed scenarios. As expected, the simulated phenomena show three main phases following classic behavior: an initiating phase characterized by fast increase in the flame height and in the horizontal flame extension from the ignition point (initiation), a long fire growth phase, a short pseudo-steady state and an extinguishing phase (decay). In the same figure, a visualization of the temperature profile at the time of flashover, intended as the time needed for the fire to reach a value of 70% of the maximum value of HRR per unit target area at 1 m downwind distance from the pool edge is also given, for the scenario involving spill of 6126 kg of fuel. Similar plots and trends are obtained for the other pools and are not reported here for the sake of brevity.

From the figure, it can be observed that, despite the large difference in HRR, the overall duration of the pool fire is weekly dependent on the amount of fuel (or pool dimension). Indeed, the pool fires extinguish in about two minutes for all the studied scenarios and boundary conditions (no differences for early and late ignition), due to the elevated mass burning rate per unit area of Jet A-1. Further details on the numerical results are given in Table 4.

In order to evaluate the fatality likelihood to the pool fire, following the methodology previously described, Fig. 15 shows the maximum heat radiation calculated at the ground level at different downwind distances from the flame surface. Based on the data reported in the figure, and assuming the threshold value for heat radiation for the fatality, injuries and for the structural damage of the equipment, it is

Table 4
Calculated pool fire duration and time to flashover for the three investigated scenarios.

Scenario	Time to flashover [s]	Fire height [m]	Maximum fire temperature [°C]
(2)	10	21.45	420
(3)	13	44.98	730
(4)	16	63.64	800

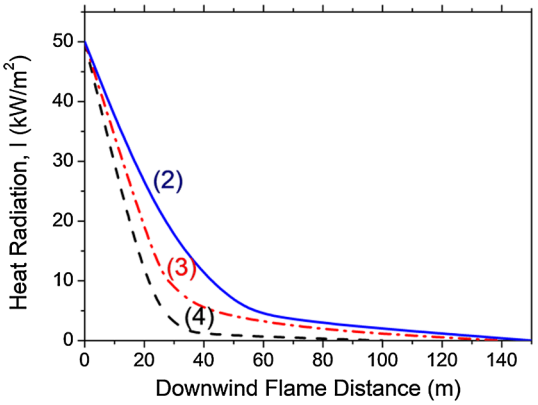

Fig. 15. Pool fire heat radiation as a function of flame distance for the three investigated scenarios.

possible to calculate the safe distance for the analyzed scenarios (Basta and Struckl, 2006). Results are shown in Table 5. Quite clearly, the stand-off distance increases with pool fire diameter with a factor of two if considering the minimum and the maximum pool extension. It is worth noting that the calculated distances refer to the flame surface at the edge of the pool diameter. All the given evaluations are identical for the late pool fire, but the ignition energy source. For the flash-fire, results are reported in Table 6.

The calculated safety distances represent the key parameters for the secondary effects, as they define the region in which, if industrial plants are present, domino effects (i.e., triggered industrial accidents) are possible. Following a simplified methodology, herein, the threshold values reported in Table 5 for the structural damage of industrial equipment, which represent a conservative choice for the domino effects, have been considered for further evaluations, as analyzed in the next section for the upgrade of the Amerigo Vespucci Florence airport.

5.5. Results of the chemical modelling for the domino effects

The three scenarios related to the release of content from the aircraft storage system or the direct impact of the crashed airplane on the industrial installation, may trigger domino. To this regard, it is important noting that industrial installations storing relevant amount of hazardous materials as per Seveso Directive (2012/19/EU, 2012) are located in the area surrounding the airport and analyzed in the study (see Fig. 10). Therefore, they have been considered for the IR assessment. Besides, buried and mounded equipment have not been considered as prone to domino effects.

The main characteristics and properties of the substances stored in the installations are given in Table 7, where the industrial facilities are

Table 5
Stand-off Distance [m] for the pool fire related to the release scenarios analyzed in this work. Threshold values for heat radiation are also reported (Basta and Struckl, 2006).

	Structural damage	Fatality	Irreversible damage (Injury)	Reversible damage (Injury)
Threshold value [kW m^{-2}]	12.50	7.00	5.00	3.00
Scenario	Distance [m]	Distance [m]	Distance [m]	Distance [m]
(2)	19.80	23.75	27.00	31.00
(3)	25.50	33.40	45.00	65.40
(4)	37.60	48.50	59.00	82.20

Table 6
Safety distance (in m) for the flash fire for the scenarios analyzed in this work.

Scenario	1/2 LFL Distance [m] (injuries)	LFL Distance [m] (fatality)
(2)	20	13
(3)	50	35
(4)	74	54

indicated with letters from A to C. For each storage tank of the facilities, when applicable, a catch basin with the same volume of the corresponding tank, has been considered for the evaluation of the pool extension.

Following the same methodology previously described for the primary scenarios, the fire phenomena (flash-fire, pool fire, fireball) and the dispersion analysis, for each substance released from each tank after the interaction with the primary scenario, have been performed using FDS. The effects of substance on individuals related to their concentration in air have been calculated by using the substance-specific *probit* coefficients as reported in CPR14E (2005) and CPR16E (2005). For the effects of heat radiation, the same equations adopted for the primary scenarios have been adopted.

6. Individual risks contours

Now that all the methods have been described, it is possible to combine the results of the aircraft dynamics and the chemical modelling probabilistic results, as per the risk-framing Eq. (11), to get the IR contours for the 2029 traffic scenario of the upgraded Amerigo Vespucci airport. These contours are given in Fig. 16, that is the annual fatality risk for the area under study (the rectangle in the figure) in the form of *iso*-risk curves.

It is noted that the maximum risk is observed along the axis of the runway, as expected. This maximum value of IR is equal to $6.6 \cdot 10^{-6}$. The IR decreases rapidly as getting away from the runway as expected from the crash contours in Fig. 10, where it falls below 10^{-8}. In fact, most of the airport area is below of this risk, while the largest IR occurs outside the airport, along the straight takeoff and landing route. Only one of the Seveso-type facilities determines a hotspot of 10^{-7} IR area. The fact that two different trajectories are available for takeoff does not produce a

Fig. 16. Individual risk (annual fatality probability contours for the 2029 traffic scenario of the upgraded Amerigo Vespucci airport.

significant change in the symmetry of risk distribution for the following reasons:

1) the two trajectories separate at a point where the altitude of aircraft is enough to reduce significantly the risk of subsequent failure standing the model reported in Fig. 7;
2) the curved, (i.e. secondary) trajectory is considered less frequent than the straight one in the procedures developed by aeronautical authorities.

7. Discussion and conclusions

This paper discussed the quantitative assessment, via analytical

Table 7
Main characteristics of the industrial installations (Ins) included in the physical domain analyzed in this case study. Hazard statement refers to the classification and labelling of chemical substances (CLP/GHS) as adopted by the European Commission.

Industrial Facility	Hazardous material	Hazard Statement	Number of Tanks	Amount [ton]
A	Acetic Acid	314–226	1	1500
	Formic Acid	226–314	1	200
	Tetrachloroethylene	315–351 – 411	1	85
	Hydrofluoric Acid	300–310 – 330–314	1	2
B	Diesel oil	226–332 – 304–315 – 319–336 – 413	2	10,000
	Gasoline	226–304–350	3	5500
C	Ethanol	225	1	20
	Liquified Petroleum Gas (LPG)	220–340 – 350	2	50

modeling, of the individual risk (i.e., the annual fatality risk for someone continuously located in a site during a year) for airport facilities, when the risk comes from the aircraft crash following a critical failure during takeoff and landing. The fatality causes considered are: (i) the impact of the airplane, (ii) the heat radiation produced by fires, following fuel spill in the crash, (iii) domino (cascading) effects due to the crash occurring within or in the vicinity of industrial facilities treating or storing large amount of hazardous materials.

The results of the analysis are expressed in form of contours of annual fatality rate (numerically equivalent to the annual fatality probability). Intermediate results are also the contours of crash probability in the area of the airport and the fatality risk due to energy radiation. The developed procedure is fully probabilistic and follows the principles of risk analysis; in addition, it required aeronautical engineering for the aircraft dynamics modelling and chemical engineering for the modeling and analysis of the radiation effects.

The risk analysis was applied to the case study of the fore coming upgrade of the Amerigo Vespucci (Florence, Italy) airport, which is undergoing major modifications, including a new and longer runway, to significantly increase its traffic by 2029. The considered aircraft for the analysis is the A320^{TM}, which is the most representative plane for the airport in the near future; however, the approach can be applied arbitrarily-composed fleet mixes. The A320^{TM} has a critical failure rate in the order of 10^{-7} per number of takeoffs and landings. The individual risk (IR) contours results for this specific airport indicate that the IR is never above $6.6{\cdot}10^{-6}$ and that it rapidly falls below 10^{-8} outside the airport area.

The working hypotheses and simplifications made in this study, not detrimental for the generality of this study, and that can be refined in further similar assessment, are briefly discussed in the Appendix A. Finally, it is believed the methodology and the case study can contribute to standardize quantitative probabilistic risk assessment tailored for specific airport facilities possibly overcoming the limitation of statistical approaches often relying on few historical data hardly exportable to specific facilities.

Acknowledgements

This study was developed thanks to the funding of Toscana Aeroporti s.p.a (TAE) to Università degli Studi di Napoli and Università di Bologna. Discussions and support from Vittorio Fanti (TAE), Lorenzo Tenerani (TAE), Massimiliano Giorgio (Università degli Studi della Campania Luigi Vanvitelli) and Gabriele Landucci (Università di Pisa) are also acknowledged.

Appendix A

Herein the working hypotheses assumed in the study are discussed. These are possibly susceptible of revisions in further studies. It is expected that the refinement of these hypotheses on the basis of knowledge leads, in general, to a reduction of the assessed risk.

A.1. Risk formulation

- The individual risk is the probability of death per year of exposure to an individual at a certain distance from the hazardous source. It is usually expressed in the form of *iso*-risk contours. In this work, the formulation assumes the constant presence (outdoor) of a person in every point of the considered area. Hence, it does not take into account, by definition, the actual urbanization. In particular, it does not consider the effective spatial density of the exposed population and the temporal variability of exposure, as well as the level of protection offered by the built environment (e.g., buildings).
- In the formulation of the risk, the failure rate, the number of movements, and all the other terms were considered constant over time and equal to the expected values at the end of the considered time horizon. This stationarity is reasonable short-term, while it is likely subject to time-variance in the long term.

A.2. Aeronautical model

- The case in which the flight status of the aircraft allowed an emergency landing attempt was neglected.
- For the determination of the impact a total lack of thrust was assumed, while in many cases the thrust is reduced. In fact, in the presence of thrust, the pilot can try to reduce the impact speed also by drawing on the energy coming from the engines.
- With reference to the model of variation of the failure rate along the trajectory, even if the model developed is similar to those of an empirical nature present in the literature, to estimate low probabilities it would be advisable rely on the reliability analyses of aircraft manufacturers.

A.3. Primary chemical effects

- The type of fuel (Jet A) used in the aeronautical field is variable. This study has adopted a chemical composition that corresponds to the highest content in aromatic components that, while remaining in international standards, leads to comparatively more intense and harmful pool fire from the point of view of human life.
- The release scenarios hypothesized in this study has assumed the immediate and complete release of all the fuel contained in the tanks of the reference aircraft, considered to be at full load, and that all the fuel forms a pool of liquid on the ground. In reality, the tanks are not necessarily completely full when taking off or landing and not all the fuel contributes to the formation of the ground pool: part of the fuel has already been consumed, part is in the combustion circuit of the aircraft, and part is retained by the tank due to incomplete damage to the tank structure.
- Meteorology (prevailing wind, atmospheric temperature, ground temperature gradients, change in weather conditions during the day) has not been evaluated. In fact, only the condition F2 (atmospheric class F, wind 2) has been considered, often considered the most conservative with respect to the extent of the dispersion of toxic and flammable materials.
- The dispersions have always been considered circular and with a radius corresponding to the maximum distance reached by toxic and flammable substances.
- The ground temperature was considered equal to 40 °C for the whole calendar year. The hypothesis is made necessary by the non-flammability of fuels for air use at temperatures lower than the one chosen. No evaluations were made on the number of hours per year in which these conditions are met, nor assessments of the thermal gradient on the ground was performed.
- As already mentioned above, the calculated local risk foresees a constant presence of a person, unprotected, in every point of the area. The possibility of protection, escape or warning has not been taken into account.
- The intervention by firefighters, mitigation and warning systems, has not been taken into account.
- Individual exposure to irradiation for pool fire, concentration for flash-fires and toxic dispersions due to domino effects, was assessed through classical probabilistic functions. In the case of irradiation and concentrations, a time equal to 1800 s, according to practice, was assumed, a value that is almost always higher than the total time of the incidental phenomenon.
- In the case of flash-fire, death is normally considered for concentrations above the upper flammability limit. Conservatively and to take into account the considerable uncertainties in the evaluation of atmospheric dispersions, in the study a value equal to half of this limit was chosen. This value represents the limit value for irreversible damage (severe burns) to the person and not to the death of the

individual (Basta and Struckl, 2006).

A.4. Domino

- The domino effects generated by the leakage of hazardous materials from containment systems (equipment, target tanks) located within relevant risk industries have been considered as certain for pool fuel fire irradiation values equal to higher than 12.5 $kW\,m^{-2}$.
- The hypotheses on the leakage, on the dispersion and on the ignition of the dangerous and/or inflammable materials out of the relative containment systems (equipment, tanks) present in the installations at risk of a major accident, have always been conservatively done. In particular, the leakage of the maximum amount of material contained in the target equipment has always been considered and the probability of death due to exposure to materials that are at the same time dangerous and flammable has always been considered, despite the almost certain ignition of the substances leaked (if flammable) from equipment close to pool fire and subjected to intense radiation.

References

2012/19/EU, 2012. Directive of the European Parliament and of the council of 4 July 2012 on waste electrical and electronic equipment, WEEE. Off. J. Eur. Union 197, 38–71.

Airbus. 2004. Getting to Grips with Aircraft Weight and Balance. http://www.smartcockpit.com/docs/Getting_To_Grips_With_Weight_and_Balance.pdf.

Airbus. 2005. Airport and Maintenance Planning Code Descriptions of Change. Customer Services, Airbus.

Airbus. 2017. A Statistical Analysis of Commercial Aviation Accidents 1958-2017. https://www.airbus.com/content/dam/corporate-topics/publications/safety-first/Airbus-Commercial-Aviation-Accidents-1958-2017.pdf.

Ale, B.J.M., Piers, M., 2000. The assessment and management of third party risk around a major Airport. J. Hazard. Mater. https://doi.org/10.1016/S0304-3894(99)00069-2.

Arros, Jorma, Doumbalski, Nikolay, 2007. Analysis of aircraft impact to concrete structures. Nucl. Eng. Des. https://doi.org/10.1016/j.nucengdes.2006.09.044.

ASTM. 2010. Standard Specification for Aviation Turbine Fuels. Annual Book of ASTM Standards. 2010. https://doi.org/10.1520/D1655-10.2.

Babrauskas, Vytenis, 1983. Estimating large pool fire burning rates. Fire Technol. 19 (4), 251–261. https://doi.org/10.1007/BF02380810.

Basta, Claudia, Michael Struckl. 2006. Implementing Art.12 of the Seveso II Directive: Overview of Procedures in Selected Member States & 'Roadmap' proposaLS." Ispra (Italy). http://www.mit.gov.it/mit/media/seveso2/pages/documents/riunini-comitato/24_02_2006/Roadmappropfinal_ver1.pdf.

Benjamin, J., Cornell, C.A., 1970. Probability, Statistics, and Decision for Civil Engineers. McGraw-Hill, New York, NY.

Blackmore, D.R., Herman, M.N., Woodward, J.L., 1982. Heavy gas dispersion models. J. Hazard. Mater. 6 (1–2), 107–128. https://doi.org/10.1016/0304-3894(82)80036-8.

Boeing. 2015. Statistical Summary of Commercial Jet Airplane Accidents.

Campedel, Michela, Cozzani, Valerio, Garcia-Agreda, Anita, Salzano, Ernesto, 2008. Extending the quantitative assessment of industrial risks to earthquake effects. Risk Anal. 28 (5), 1231–1246. https://doi.org/10.1111/j.1539-6924.2008.01092.x.

CCPS, 2010. Guidelines for Evaluating the Characteristics of Vapor Cloud Explosions, Flash Fires, and BLEVEs. The Center for Chemical Process Safety, American Institute of Chemical Engineering, John Wiley & Sons.

COMAH, 2015. Control of Major Accident Hazards Regulations, Health and Safety Executive, SI 2015/483.

Commission, European. 2015. The European Aviation Safety Programme {COM(2011) 670 Final}." SEC(2011) 1261. Brussels, Belgium. https://eur-lex.europa.eu/LexUriServ/LexUriServ.do?uri=SEC:2011:1261:FIN:EN:PDF.

Coordination Committee (CCOM) for the US-EU MoC Annex 1 High-Level Committee. 2014. State of Harmonisation Document. https://www.sesarju.eu/sites/default/files/State-of-Harmonisation.pdf.

Cozzani, Valerio, Salzano, Ernesto, 2004a. The quantitative assessment of domino effect caused by overpressure: Part II. Case studies. J. Hazard. Mater. 107 (3), 81–94. https://doi.org/10.1016/J.JHAZMAT.2003.09.014.

Cozzani, Valerio, Salzano, Ernesto, 2004b. The quantitative assessment of domino effects caused by overpressure: Part I. Probit models. J. Hazard. Mater. 107 (3), 67–80. https://doi.org/10.1016/J.JHAZMAT.2003.09.013.

Cozzani, Valerio, Salzano, Ernesto, 2004c. Threshold values for domino effects caused by blast wave interaction with process equipment. J. Loss Prev. Process Ind. 17 (6), 437–447. https://doi.org/10.1016/J.JLP.2004.08.003.

CPR14E, 2005. Methods for the Calculation of Physical Effects – Due to Releases of Hazardous Materials (Liquids and Gases). The Hague (NL).

CPR16E, 2005. Methods for the Determination the Possible Damage. The Hague (NL).

Davies, P.A., Quinn, D.J., 2004. Airport public safety zones: Part 2 — Risk Model application. In: Probabilistic Safety Assessment and Management. Springer London, London:, pp. 242–247.

Drysdale, Dougal, 2011. An Introduction to Fire Dynamics. John Wiley & Sons, Ltd, Chichester, UK.

EASA. 2007. Certification Specifications for Large Aeroplanes CS-25.

Eddings, Eric G., Yan, Shihong, Ciro, William, Sarofim, Adel F., 2005. Formulation of a surrogate for the simulation of jet fuel pool fires. Combust. Sci. Technol. 177 (4), 715–739.

Erto, P., Giorgio, M., Iervolino, I., 2016. About knowledge and responsibility in probabilistic seismic risk management. Seismol. Res. Lett. 87, (5). https://doi.org/10.1785/0220160001.

EUROCONTROL. 2015. European ATM Master Plan 2015, 140. https://doi.org/10.2829/240873.

FAA. 2012. Technical Standard Order C201 Attitude and Heading Reference Systems (AHRS).

FAA. 2016. Airplane Flying Handbook, Chapter 17: Emergency Procedures. In: U.S. Federal Aviation Administration. https://www.faa.gov/regulations_policies/handbooks_manuals/aviation/airplane_handbook/media/19_afh_ch17.pdf.

FAA. 2017. Aviation Safety Information Analysis and Sharing System ASIAS.

Fabbrocino, Giovanni, Iervolino, Iunio, Orlando, Francesca, Salzano, Ernesto, 2005. Quantitative risk analysis of oil storage facilities in seismic areas. J. Hazard. Mater. https://doi.org/10.1016/j.jhazmat.2005.04.015.

Fasano, G., Accardo, D., Tirri, A.E., Moccia, A., De Lellis, E., 2015. Radar/electro-optical data fusion for non-cooperative UAS sense and avoid. Aerosp. Sci. Technol. 46. https://doi.org/10.1155/2013/748751.

Glassman, Irvin, Yetter, Richard A., 2008. Combustion. Combustion. https://doi.org/10.1016/B978-0-12-088573-2.X0001-2.

Hale, A., 2002. Risk contours and risk management criteria for safety at major Airports, with particular reference to the case of Schiphol. Saf. Sci. 40 (1–4), 299–323. https://doi.org/10.1016/S0925-7535(01)00051-0.

Hottel, Hoyt C., 1959. Certain laws governing the diffusive burning of liquids-a review. Fire Res. Abstract Rev. 1, 41–44.

ICAO. 2009. Required Navigation Performance Authorization Required (RNP AR) Procedure Design Manual. Montreal, Quebec, Canada. https://www.icao.int/Meetings/PBN-Symposium/Documents/9905_cons_en.pdf.

Mahony, Sharon. 2014. Eurocontrol Specification for Collaborative Environmental Management (CEM) Specification for Collaborative Environmental Management (CEM).

Mannan, S. 2012. Lees' Loss Prevention in the Process Industries: Hazard Identification, Assessment And Control: Fourth Edition. Lees' Loss Prevention in the Process Industries: Hazard Identification, Assessment and Control: Fourth Edition. https://doi.org/10.1016/C2009-0-24104-3.

McGrattan, Kevin, Miles, Stewart, 2016. Modeling fires using computational fluid dynamics (CFD). In: SFPE Handbook of Fire Protection Engineering. Springer New York, New York, NY, pp. 1034–1065.

Nuic, Angela. 2017. User Manual for the Base of Aircraft Data (BADA) – Revision 3.13. EUROCONTROL, EEC Note No.10/17.

Oster, Clinton V., Strong, John S., Kurt Zorn, C., 2013. Analyzing aviation safety: problems, challenges, opportunities. Res. Transport. Econom. 43 (1), 148–164. https://doi.org/10.1016/j.retrec.2012.12.001.

Paltrinieri, N., Dechy, N., Salzano, E., Wardman, M., Cozzani, V., 2013. Towards a new approach for the identification of atypical accident scenarios. J. Risk Res. 16 (3–4), 337–354. https://doi.org/10.1080/13669877.2012.729518.

Paté-Cornell, Elisabeth, 2002. Risk and uncertainty analysis in government safety decisions. Risk Anal. https://doi.org/10.1111/0272-4332.00043.

Reichmuth, J., Berster, P. 2018. Past and Future Developments of the Global Air Traffic 2. 1 Introduction – Global Development in Air Transport. https://doi.org/10.1007/978-3-662-53065-8_2.

Salzano, Ernesto, Basco, Anna, Busini, Valentina, Cozzani, Valerio, Marzo, Enrico, Rota, Renato, Spadoni, Gigliola, 2013. Public awareness promoting new or emerging risks: industrial accidents triggered by natural hazards (NaTech). J. Risk Res. 16 (3–4), 469–485. https://doi.org/10.1080/13669877.2012.729529.

Spitzer, Cary, Uma Ferrell, Thomas Ferrell. 2015. Digital Avionics Handbook. Aerospace America.

De Waal, J.A., Muntendam-Bos, A.G., Roest J.P. 2015. Production Induced Subsidence and Seismicity in the Groningen Gas Field – Can It Be Managed? 3721295194 (10). 129–139. https://doi.org/10.5194/piahs-372-129-2015.

Wen, J.X., Kang, K., Donchev, T., Karwatzki, J.M., 2007. Validation of FDS for the prediction of medium-scale pool fires. Fire Saf. J. 42 (2), 127–138. https://doi.org/10.1016/J.FIRESAF.2006.08.007.

Wong, D.K.Y., Pitfield, D.E., Caves, R.E., Appleyard, A.J., 2009. The Development of a more risk-sensitive and flexible Airport safety area strategy: Part I. The development of an improved accident frequency model. Saf. Sci. 47 (7), 903–912. https://doi.org/10.1016/j.ssci.2008.09.010.